

**Investigation of equipment  
and processes that limit  
photon echo signal processing**

Andreas Walther

Master's Thesis  
LRAP - 318, LTH, March 2004

## Abstract

A number of applications of photon echoes, such as pulse compression and data storage, have been explored previously here in Lund with good results. The limiting factors in many of the cases, however, have been the characteristics of the laser system in terms of e.g. laser stability and output power. A goal in this Master's Thesis is to push those limits further towards the theoretical limitations of these techniques using improved equipment. A new diode laser constructed for this purpose is used together with a laser amplifier in order to gain a higher intensity while maintaining a narrow linewidth.

Reaching the limits of this new system a natural second goal is to better determine what exactly those limits are and if it is possible to improve them further in some way.

In the pulse compression experiments different limiting factors, such as non-linearities, were investigated. A maximum compression of a factor of 1200 was also reached for an optical pulse, which was an improvement from the previous experiments here in Lund where a factor of 450 was reached. Less time was spent on data storage but comparisons with other experiments for some parameters suggested that while laser stability has been improved, it is still one of the limiting factors.

## **Contents**

<b>1. Background</b>	<b>4</b>
<b>2. Theory</b>	<b>5</b>
2.1 Photon echoes	5
2.2 Pulse compression	9
2.3 Data storage	10
<b>3. Experiments</b>	<b>13</b>
3.1 Description of the equipment	13
3.1.1 The master laser	13
3.1.2 The laser amplifier	13
3.1.3 The acousto-optic modulators	14
3.1.4 Optical equipment	15
3.1.5 Waveform generator and oscilloscope	15
3.2 The photon echo material	16
3.3 Experimental set-ups	16
3.3.1 Pulse compression	17
3.3.2 Data storage	17
<b>4. Results and discussion</b>	<b>19</b>
4.1 Optimisation of the amplifier	19
4.2 Pulse compression	20
4.2.1 Constant chirp rate	20
4.2.2 Constant pulse duration	21
4.2.3 Adding deformations to the chirp	23
4.2.4 Laser power dependence	25
4.2.5 High compression echoes	27
4.3 Data storage	28
4.3.1 General parameters	28
4.3.2 Comparison to previous work	30
4.3.3 Final test on data storage	32
<b>5. Conclusion</b>	<b>33</b>
<b>6. Acknowledgements</b>	<b>34</b>
<b>7. List of references</b>	<b>35</b>
<b>8. Appendix A</b>	<b>36</b>

# 1. Background

There are many applications to photon echoes. It is for example possible to compress an optical pulse from a laser by chirping the laser frequency and using certain properties of the photon echo material, as will be described in the following chapter.

Another technique where photon echoes can be applied is to store a sequence of optical pulses for a certain time, and then recall them, i.e. optical data storage. One spatial storage point in the photon echo material is limited by the focus of the laser beam, but it is then possible to store several bits in such a point by using a different frequency interval for each bit. How this works will be explained in the theory section of this thesis, but it can be said that there are materials that allow up to  $10^7$  spectral channels in every spatial point.

A few of years ago this method was comparable to conventional storage media, such as CD's, that are also optical, and hard drives, which are magnetic mediums. Today magnetic storage at almost  $10 \text{ Gbit/cm}^2$  is readily available commercially, which is an order of magnitude above the  $1.2 \text{ Gbit/cm}^2$  that has been done with photon echoes in [1]. It was estimated in [1] that data storage with photon echoes could reach capacities up to  $15 \text{ Gbit/cm}^2$ , but experimental difficulties have halted the progress.

The most promising area of research for photon echoes right now is signal processing. Already there are commercial systems being developed with applications in e.g. radar technology.

It is interesting to note that the same materials that are being used for photon echoes, rare-earth crystals, are also being used to realise quantum computers by the photon echo group here Lund, where this thesis was done. These rare-earth quantum computers use the same properties as the photon echo process, and it can therefore be of value to investigate these materials thoroughly.

The main objective with this thesis however, is to test some new equipment constructed by the photon echo group in Lund. Both pulse compression and optical data storage have been done here in Lund before, but since then a new laser has been constructed with properties specifically designed for photon echo experiments.

Besides that, a laser amplifier has also been constructed to increase the beam power, while keeping a narrow line width. As will be explained in the thesis, the intensity of photon echoes depends strongly on the intensity of the incoming beam. The expectations are that this increase in power can improve the results compared to previous experiments.

## 2. Theory

### 2.1 Photon echoes

The general description of what happens in the normal 2-pulse photon echo is basically: you send in two laser pulses separated by some time  $T$  into a material with certain properties. Then at time  $T$  after the second pulse the material will send out a third pulse, the echo, propagating in the same direction as the 2 incoming pulses.

The material in our case is a homogeneous crystal doped with a small concentration of ions located in random positions in the crystal. Because of this randomness in position of the doped ions the individual resonance frequencies of the ions will be shifted slightly depending on for example how far away the neighbouring doped ions are. This creates an inhomogeneous absorption profile. Favourable material properties, in order to create photon echoes, should be a narrow homogeneous linewidth for each transition, and yet many different resonance frequencies creating a broad inhomogeneous linewidth.

In order to correctly describe the process of creating an echo, we need to use the theory provided by quantum mechanics. We will consider a number of systems (atoms or molecules), an ensemble, with two energy levels each. These systems are characterised by a ground state, denoted  $|g\rangle$ , that has an energy of zero and an excited state, denoted  $|e\rangle$ , that has an energy of  $E = \hbar\omega$ . One such system can be described by the wave function:

$$|\psi\rangle = c_g(t)|g\rangle + c_e(t)|e\rangle \quad (1)$$

Here the square of the complex coefficients  $c_g$  and  $c_e$  gives the probability of finding the system in the corresponding state, as a function of time, when measured. Conservation of probability gives the relation  $|c_g(t)|^2 + |c_e(t)|^2 = 1$ . Classically we would expect to find an atom either in the ground state or in the excited state, but the theories of quantum mechanics has explained how also superpositions of these states are allowed. If the coefficients in (1) are  $c_g^2 = c_e^2 = 1/2$  for example, the atom exists in a composite state with equally large contributions from both eigenstates. As soon as we perform a measurement on the system, however, it will be found in one of the two states with a probability of 50 % for both states. This will collapse the superposition and after the measurement the atom will be in the measured state with a probability of 100 %.

Interaction with the system is done with laser light. A laser pulse can be expressed as:

$$E(r,t) = E_0 e^{i(\mathbf{k}\cdot\mathbf{r} - \omega_0 t)}, \quad (2)$$

where  $\omega_0$  is the angular frequency of the light and  $\mathbf{k}$  is the wave vector describing the direction of propagation. Light that is resonant with the system ( $\omega_0 \approx \omega$ ) can change the amplitude coefficients, that is it can stimulate the system to absorb or emit light, depending on the relative phase of the light and the system. The complete treatment of this is a bit too long to include here so only the results are given, but more on this can be found in e.g. [2].

If the system is in the ground state from the beginning, the new amplitudes after the interaction are given by (if we don't include the global phase):

$$\begin{aligned} c_g(t_1) &= \cos(\theta/2) \\ c_e(t_1) &= ie^{-i\varphi} \sin(\theta/2) \end{aligned} \quad (3)$$

where  $t_1$  is the duration of the laser pulse,  $\varphi$  the phase relative some chosen zero point, and  $\theta$  is called the pulse area. It is defined as:

$$\theta = \frac{\mu \cdot E_0}{\hbar} t_1 \equiv \Omega_R t_1, \quad (4)$$

where  $\mu$  is the electrical dipole transition moment between the ground and the excited state. It is assumed that the electrical field  $E_0$  is constant during  $t_1$  and that the laser frequency equals the resonance frequency. The Rabi frequency,  $\Omega_R$ , is sometimes used as shown.

To create an optimally strong echo each atom need to be in the superposition  $c_g^2 = c_e^2 = 1/2$ . The equations in (3) show that this can be accomplished by a pulse area of  $\theta = \pi/2$ . Similarly a  $\pi$ -pulse completely flips the state so that the system goes for example from the ground state into the excited state.

A good visualisation of how the light interacts with the system can be gained by using the Bloch sphere. In this theory the state is represented by a vector that lies on this sphere, as can be seen in figure 2.1 below.

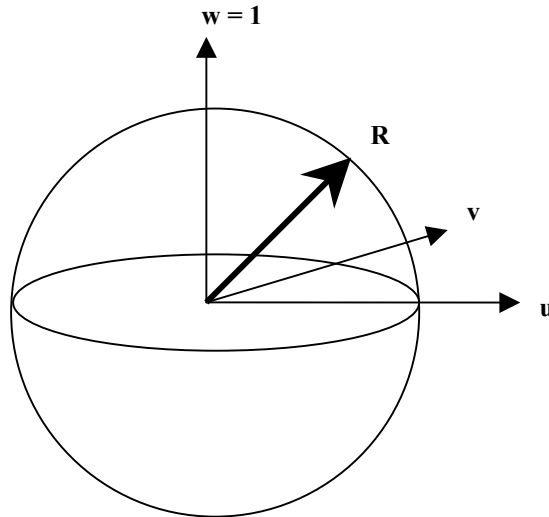


Figure 2.1. An arbitrary phase/amplitude vector,  $\mathbf{R}$ , inscribed in the Bloch sphere.

Here a value of  $w = -1$  represents the atom being in the ground state and  $w = 1$  is the excited state. The  $(u,v)$ -plane perpendicular to the  $w$ -axis shows the relative phase factor,

also given in eq. (3), between the probability amplitudes of the states. The previously mentioned  $\pi$ -pulse for example, would rotate the vector  $180^\circ$  from  $w = -1$  to  $1$ .

An ion has a certain charge distribution because the electron of the transition of interest has a certain probability distribution described by the wave function. For an ion in a superposition of states this charge density varies with time and creates an oscillating dipole moment, which in turn will emit radiation with intensity proportional to the number of ions. In e.g. [3] it is found that the angular speed of this oscillation is equal to  $\omega$ , that is the energy difference between the ground state and the excited state divided by  $\hbar$ . As mentioned all the ions have slightly different transition frequencies and this will mean that the phase of the dipole moment oscillation will develop with different speeds for all systems.

To create an optimal echo, the first pulse should have a pulse area of  $\pi/2$ . This would rotate the initial state from  $w = -1$  up to a superposition described by the vector being in the  $(u,v)$ -plane, with  $w = 0$ . When the state is first excited by the light, all the systems (ions) in the material used are put in the same phase relative to the phase of the laser field. However, not all of the systems have the exact same resonance frequencies as mentioned and as the phase of the superposition develops in time the off-resonance systems will dephase with respect to the in-resonance ones. Putting the vectors from many two-level systems in the same Bloch sphere this can be described as a spreading in the  $(u,v)$ -plane (the phase plane) as seen in figure 2.2a below. In general all the systems resonance frequencies differ from the laser frequency by different amounts and thus they will spread from the initial phase with different speeds, that is rotate around the  $w$ -axis with different angular velocities. The effect of the second pulse ( $\pi$ -pulse) is to turn the phase  $180^\circ$  in the  $(u,v)$ -plane, that is to flip all the vectors around the  $v$ -axis as shown in figure 2.2b. As the direction of rotation (clockwise or counter clockwise) is due to whether they are above or below the non-shifted frequency, and thus does not change in this operation, they will now start to rephase again.

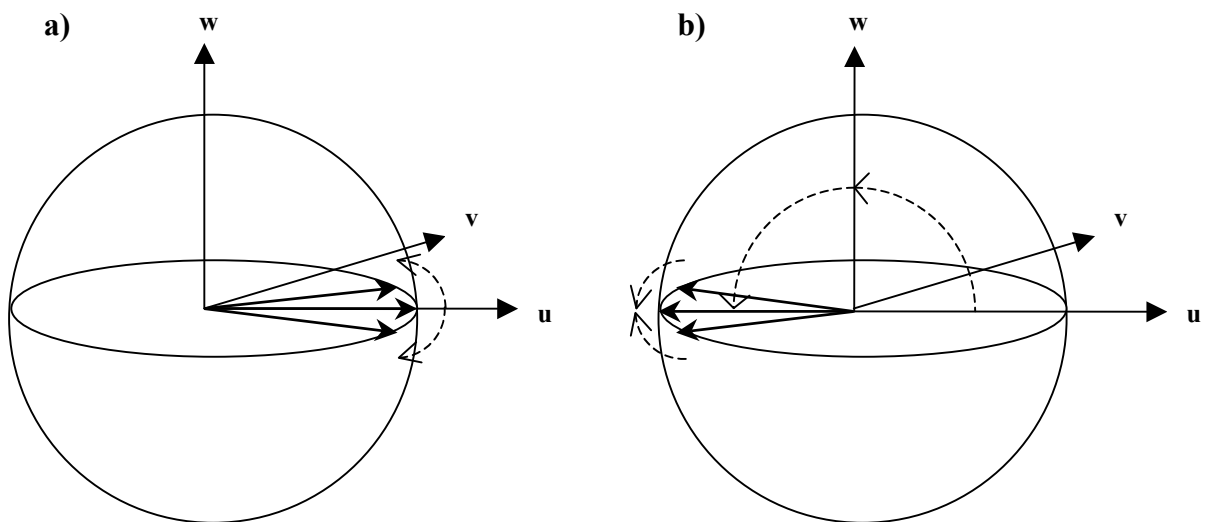


*Figure 2.2 The solid arrows inside the sphere represent the state vectors from many two-level systems, and the dotted arrows show how these states are moved. a) Ions slightly off the resonance frequency will spread out in the phase plane of the sphere. b) After the phase shift of  $180^\circ$ , as they still keep their direction of rotation, they will start moving towards being in phase again.*

If the  $\pi$  pulse came the time  $T$  after the first pulse then phases will coincide again the same time  $T$  after the second pulse, and it is this that will produce the echo. All the oscillations add up and macroscopically this can be seen as interfering fields. Only where the interference is constructive will an echo appear, and the intensity will then be proportional to the number of oscillating dipoles squared. For emission of radiation all these individual light sources need to emit not only in phase but also in the same direction. This can also be expressed as a conservation of momentum. Written in wave vectors:

$$\mathbf{k}_e = 2 \cdot \mathbf{k}_2 - \mathbf{k}_1, \quad (5)$$

where  $\mathbf{k}_1$  and  $\mathbf{k}_2$  are the wave vectors of the two incoming pulses and  $\mathbf{k}_e$  is the wave vector of the echo. If both the incoming pulses are in the same direction then it follows that the echo will also be in this direction.

The theory above explains the 2-pulse echo, and the following section will describe the more general three pulse echo. As the emission of coherent radiation requires that the coherence of the states have to be preserved during the entire course of events, the two pulses and the echo have to be within the coherence time of the excited state. However, as all the ions oscillate with a different frequency, they will be in a different phase when they are effected by the second light pulse. Some ranges of frequencies will be out of phase with the light and they will absorb light, thus getting excited. The other ions will be roughly in phase and they will de-excite, emitting light in the process. Of course not all ions are precisely in or out of phase, but rather a somewhere in between. This can make the description very complicated so it will be sufficient to say that the net effect is that the out of phase ions will be more excited than the in phase ones. The excited ions now all belong to certain periodic frequency intervals. A frequency grating stored as a population difference in the states has been created. This will last as long as the lifetime of the excited state, which can be much longer than the coherence time. If, some time after the second pulse, a third pulse comes, it can put the ions back in the superposition they where in after the second pulse. The time,  $T$ , between the first two pulses will be stored in the spectral grating, and this time  $T$  after the third pulse a 3-pulse echo, a stimulated echo, will appear. As used later in this thesis, this can be expanded to explain how a sequence of pulses can be stored as a more complex grating. The relation between the time separations and the frequency spacing of the spectral grating is essentially a Fourier transform, which can be described by the relation  $\Delta f \sim 1/\Delta T$ .

The phase matching conditions of a 3-pulse echo can be expressed as:

$$\mathbf{k}_e = \mathbf{k}_3 + \mathbf{k}_2 - \mathbf{k}_1 \quad (6)$$

The 2-pulse echo is actually a special case of the 3-pulse echo, where the second pulse acts both as second and third pulse. It is easy to verify that equation (5) is received when letting  $\mathbf{k}_3 = \mathbf{k}_2$  in eq. (6) here above.

In our crystal however, the excited state can relax not only back to the ground state but also to a third, metastable state. There is an approximately equal chance for the excited states to decay to the metastable state or to the ground state. The ones that decay back to the ground state will start to fill up the frequency holes created after the second pulse and this will diminish the amplitude of the echo. But since the rest decay to the metastable state, there

are still fewer ions in the ground state in certain frequency intervals. This can be used to store the spectral grating for an even longer time period, as the lifetime of a metastable state is usually fairly long.

## 2.2 Pulse compression

One of the applications for photon echoes is to use it to compress pulses in time. This can be accomplished by chirping the frequency of the light during the pulses. As mentioned in the general theory above the material stores the time between the two pulses. By chirping the second pulse faster than the first, it is possible to control all the small echoes from different frequency components in the chimp, to emit light at the same time, as figure 2.3 describes:

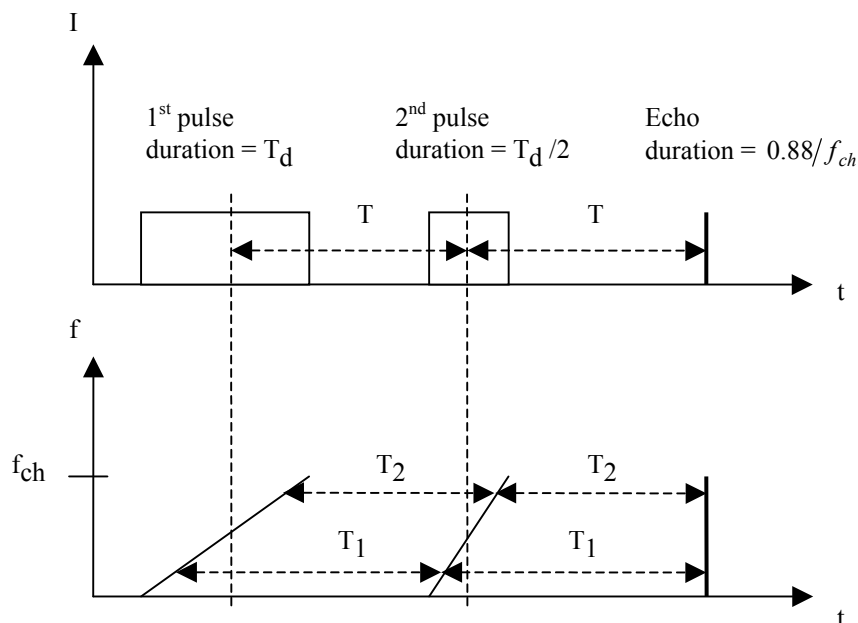


Figure 2.3 Temporal compression of an echo is done by chirping the two pulses in frequency and by letting the second pulse be chirped twice as fast. One can see from the lower part that the time from the first pulse to the second is always the same as that from the second to the echo, but that it is different for each frequency component.

It can be seen in figure 2.3 that the second pulse must be correspondingly shorter than the first. An analytical treatment of this process can be found in e.g. [4] and there it is shown that the best compression is done when the second chirp is exactly twice as fast as the first. Looking at the creation of a compressed echo in the frequency plane one sees that it is the collective effect of a several different frequencies interfering constructively at the centre of the echo and destructively for the rest. Knowing this it is not surprising to learn that the duration of the compressed echo is inversely proportional to the bandwidth,  $f_{ch}$ , used in the chirp. In other words, the more frequency channels you incorporate into the pulse the more pronounced the interference effects would be. Square pulses have been used in this thesis and an analytical treatment of this (again from [4]) shows that the shape of the echo can be described as a sinc function. With  $t$  chosen to be zero at the centre of the echo intensity,  $I$ :

$$I(t) \propto \text{sinc}^2(\pi f_{ch} t) \quad (7)$$

From this it is possible to give a theoretical evaluation of what the FWHM of the echo would be. The FWHM of the compressed echo is:

$$T_e \approx 0.88 \cdot \frac{1}{f_{ch}} \quad (8)$$

This result shows what was previously discussed, the larger frequency range of the chirp the shorter the echo will be.

Deformed shapes of the echo can occur if the chirping speeds aren't quite right, say for example that it isn't completely linear but have some quadratic term to it. Ideally for the pulse compression the frequency as a function of time would be the shift  $r_{ch} \cdot t$  added to a starting frequency  $f_0$  but a quadratic non-linearity would look like:

$$f(t) = f_0 + r_{ch}t + Lt^2 \quad (9)$$

where L is a constant that determines the strength of the quadratic term. Arguing that the effect of the quadratic term will start to show if the quadratic chirp deviates more in time from the linear chirp than the FWHM of an echo created without this deformity, one can find an analytical expression for at what value of L this effect will be noticeable. This is done in [4] where it is found that  $L_{limit} = \frac{22}{T^3}$ , where  $T$  is the pulse length.\*

## 2.3 Data storage

Another application of photon echoes has already been mentioned, namely the possibility to store a whole train of pulses. The most intuitive way of doing this is with what is called time-domain data storage. Here the first pulse for creating an echo, the reference pulse, is a strong  $\pi/2$  pulse just as before, and then the whole train of pulses, data pulses, is sent into the material. These have to be of much lesser amplitude than the reference pulse so that the main interaction for each data pulse is between that pulse and the reference pulse, and not between one data pulse and another. As the reference pulse governs when data will be written, it will often be called write pulse in data storage experiments.

The sequence of light pulses carries a certain phase and amplitude that has a characteristic Fourier transform. This Fourier transform will, just as in the single pulse case, be stored in the population of the states as a frequency grating. It is desirable to make the duration of the first pulse short in time, so that it will be broad in frequency, because the more of the inhomogeneous bandwidth is used, the more frequency channels can be used for the storage. Looking at the pulse area in eq. (4) it can be seen that the shorter the pulse is made the larger the amplitude of the electric field must be, in order to obtain the optimum pulse area of  $\pi/2$ . This means a larger intensity is required, and since the laser intensity is limited, there is also a limit as to how short pulses, and thus how much bandwidth, can be used here. Another limitation is that the entire sequence must be written within the coherence time of the excited state, as the phases must be remembered.

---

\* Note that L in this thesis differs from the L in Afzelius work [3] by a factor of 3 due to different definitions.

Some of these limitations to the time-domain data storage can be overcome by chirping the frequency of the laser just as described in the pulse compression section. This is called swept carrier time-domain data storage (introduced by Mossberg in [5]) and here different data bits will be stored in different spectral regions. Instead of having one short pulse as the first pulse, the reference pulse, or write pulse, is here a long pulse that covers the inhomogeneous bandwidth by chirping instead of by the Fourier width as for the short pulse. By letting the reference pulse and the data pulses be sent into the material by two beams instead of one it is possible to write the data sequence while the reference is still on. This is done by letting the different beams be shifted in frequency in respect to each other. The third pulse, the read pulse, should be a copy of the reference. Figure 2.4 explains the events:

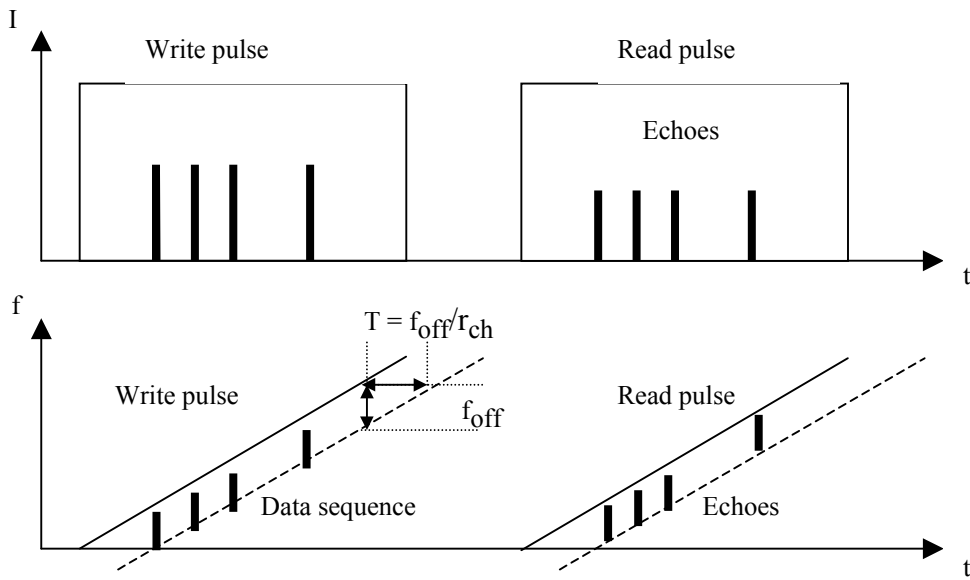


Figure 2.4 The data sequence is starting to be written before the write pulse has ended. The lower picture shows how the frequency of the two beams are chirped. The time between write and the data beams is governed by how much the frequency offset is and how fast the chirp is swept.

The separation between the write and the data beam,  $T$ , will be governed by the size of the frequency offset,  $f_{off}$ , between the beams and the chirp rate,  $r_{ch}$ , according to  $T = f_{off} / r_{ch}$ . This time follows the same restrictions as the corresponding time between the first and second pulse as before in the basic 3-pulse echo. It means for example that  $T$  has to be smaller than the coherence time of the excited state.

For ease of notation later on we will here define some more parameters.  $\Delta t_b$  will be used as the time separation between the bits and  $t_{wr}$  will be the time between the write pulse and the read out pulse. If the duration of one of the data pulses (a bit) is  $t_b$ , then it will have a corresponding width in the frequency plane described approximately by  $\Delta \nu \approx 2/t_b$ , as the data pulses are square pulses. Also if the chirp rate is  $r_{ch}$  and total duration of the sequence is  $t_{seq}$ , then the total frequency interval used will be  $f_{tot} = r_{ch} \cdot t_{seq}$ . Divided by the number of bits used in the sequence, the frequency per bit,  $f_b$ , can be compared to the spectral width each bit has. If  $f_b$  is greater than  $\Delta \nu$ , then every bit is stored in a separate spectral channel.

If not then they will overlap in frequency. This might cause a problem as it sets harder restrictions on the coherence of the laser. If they are completely separate in frequency then it doesn't matter if the laser shifts in phase between bits. Now, if they overlap, since the laser should be coherent during the whole of one bit, and the next bit starts before the last one had ended it follows that the laser should be coherent during the whole sequence. This is often too hard a demand since it would really limit the sequence length. If the phase of the laser shifts slightly during a bit, it will be seen as a decrease in amplitude of the signal. This said, it should be noted that nothing in particular happens precisely at the point where they begin to overlap. It is rather a continuing process where it becomes increasingly probable for the laser to phase shift during one bit the smaller the separation are in frequency between bits. One must also make sure the frequency offset between the beams is at least larger than  $\Delta\nu$ , or else the data pulses will have a wide enough spread to access frequency ranges that have not yet been covered by the write beam.

It is also possible to combine the two applications described and create a temporal compression of sequence of bits. It is not a strange procedure, one just chirps the read pulse twice as fast as the reference pulse for optimal compression, as before.

## 3. Experiments

### 3.1 Description of the equipment

In this section the lasers and other equipment will be described in more detail. Later sections will then present schematics of how these components are used in the different experiments as well as a description of the photon echo material.

#### 3.1.1 The master laser

The master laser in these experiments is an external cavity diode laser constructed at LTH as another master's thesis [6]. It has a linewidth of about 300 kHz and can be mode-hop free tuned over more 10 GHz. The chirp is created in an electro-optic modulator (EOM) inside the cavity. The EOM is a crystal that slightly changes its refractive index when a voltage is applied. This will cause a change in the optical path length through the cavity, and thus change what wavelength will be amplified. It has been tested to give a linear response according to 13.5 MHz/V. The output power of this laser is approximately 30 mW.

The laser diode chip was driven by a Profile LDC 202 controller and the temperature stabilisation was controlled by a Profile TED 200. There is also a possibility to temperature stabilise the base plate, but it was found not to be needed during the experiments.

#### 3.1.2 The laser amplifier

The photon echo is a third order process as seen if the susceptibility tensor for this process is derived. The details of this will not be presented here but can be found in e.g. [7], which give a description of the echo process known as the Fourier model. It means that the electric field of the output echo will be proportional to the cube of the laser field in use. Knowing this we can understand why higher laser intensity is desirable in photon echo experiments. One of the main ideas in this thesis is to improve results by using a laser amplifier to boost the output from a master laser, which in the present case is a diode laser. The amplifier is also a diode laser in itself but capable of much higher output powers than the master laser. The difference between the two is that the amplifier is a broad area diode laser, which because of its large volume has large inverted population. This together with an anti reflection coat decreases the amplifiers own lasing while still enabling a good gain for an injected beam. The master laser on the other hand is an external cavity diode laser specifically designed to meet the requirements of photon echo experiments, such as narrow single mode linewidth and possibility to make fast and accurate sweeps over a broad frequency range. When the master laser beam is injected into the amplifier the effect will be that the incoming beam is enhanced rather than that the amplifier will lase on it's own. Thus the output from the amplifier will be a beam that has the good spatial and spectral properties of the original beam, but has gained power from passing through the amplifier diode chip.

Of course there are some spontaneous emissions in the amplifier that will cause some components in the output beam to be of other frequencies than desired. This Amplified Spontaneous Emission (ASE) will be checked during the experiments to verify that it is a very small part of the beam.

The amplifier used in these experiments was constructed at LTH as a master's thesis [8]. It uses a double pass technique, which means that the beam from the master laser comes in at one end at some angle, reflects at the other end and exits the same end it came in. This uses a fairly large part of the diode chip, but not all, as drawn in figure 3.1. It is also relatively easy to separate the ASE (Amplified Spontaneous Emission) from the amplified injection beam.

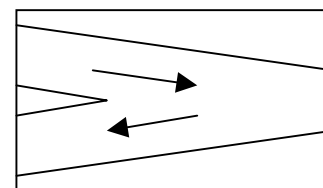


*Figure 3.1 In the double pass amplifier the incoming beam is injected at some angle.*

The output power of the amplifier itself is more than 500 mW but in order to preserve a good spectral purity of the output beam when injected, the output power in the experiments was never more than 140 mW. This is a gain of more than a factor of 4 compared to the beam without amplifier.

The amplifier was controlled by an SDL-824 driver and the temperature stabilised by equipment built here at LTH. It should be mentioned that from the designs of the amplifier given in [8] the holder for the cylindrical lens has been changed, so that it is now mounted on a rotatable holder (see appendix A for a schematic of the lens system). The incoming beam is focused through a couple of lenses onto the diode chip in the amplifier. This can be a very tricky process as the chip is only  $100 \times 1 \mu\text{m}$  in size. A lot of time were spent on getting an amplified signal at all out from the injected beam and therefore a guide for adjusting the amplifier has been included in appendix A. A more detailed description of the amplifier, including the lens system, is also given in the appendix.

### 3.1.3 The acousto-optic modulators

For the temporal modulation, that is for the creation of pulses from the continuous laser beam, acousto-optic modulators (AOM's) were used. When an electrical pulse is applied to an AOM it produces an acoustic wave through its body, effectively changing the refractive index of the AOM crystal. The voltage to the AOM is typically modulated with a frequency of 100 MHz and this produces a grating in the crystal which diffracts the laser light passing through it into several possible orders, just like from multi slit experiments. Looking at this from a particle point of view, it can be seen as the photons absorbing or emitting phonons to the acoustic wave in the crystal, so the light diffracted to the first order would have absorbed one phonon, the second two etc.

In theory it is possible to let all the incoming light be diffracted to the 1<sup>st</sup> order but experimental conditions, such as the size of the beam cross section, reduces efficiency down to about 50 % for our experiments. It is the first order light that is used in the experiments and when then modulation to the AOM is turned off, a suppression of the light of about 1000:1 was received. Suggestions were made to have two AOM's in a row to further increase the suppression, but since each AOM degrades the beam quality as well as cuts away 50 % of the light, the idea was never tried.

The AOM's have a rise time of about 100 ns and also, since it's based on the travelling of an acoustic wave, they have a delay of about  $1.2 \mu\text{s}$  as measured during the experiments. The frequency of the light coming out from the AOM has been shifted by the frequency of the phonon.

All of the AOM's used in the experiments were ISOMET 1205C Bragg cells and modulated by ISOMET D322B RF drivers.

### 3.1.4 Optical equipment

Between the master laser and the amplifier an optical isolator have to be placed to keep light from the amplifier from disturbing the master laser. The isolator is from Optics For Research (OFR, IO-5-793-HP) and has been set to have its highest transmission at 793 nm, which is the wavelength used in the experiments. The working idea for the isolator is to first have a polarisator, then a Faraday rotator and then another polarisator plate. The Faraday rotator rotates the polarisation of the incoming light by  $45^\circ$  so the exit polarisator should have be at  $45^\circ$  in respect to the first in order to let light completely ( $>92\%$ ) through. In contrast to ordinary half-wave plate the Faraday rotator rotates the light in the same direction independently of the direction of propagation of the light. This will cause light that enters from the exit polarisator to rotate so that the polarisation is completely perpendicular to first polarisator plate, thus effectively blocking the light. Measurement during the experiments showed that the suppression in the backward direction was about a 1000:1.

Just after the master laser there is an anamorphic prism. It is there to adjust the beam shape from a rather elongated elliptic shape that the master laser gives to a more circular shape. An anamorphic prism is basically two prisms separated by some distance and tilted some angle in respect to each other, which allows the size of one lateral dimension to be changed without changing the other. The scheme can be seen in figure 3.2.

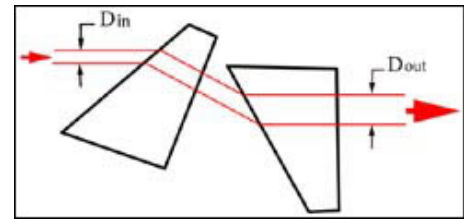


Figure 3.2 The scheme of an anamorphic prism.  $D_{in}$  and  $D_{out}$  is the respective beams diameters.

Other optical equipment in use was devices to measure wavelengths. The main Wavelength meter was a Burleigh but also a fibre spectrograph (MS257) from Oriel Instruments was used when optimising the amplifier.

### 3.1.5 Waveform generator and oscilloscope

To control the AOM's to give a desired pulse sequence a TGA1244 Arbitrary Waveform Generator was used. It runs on a 40 MHz clock and can be programmed from a computer. A thought at one time was that the step size in time provided by a 40 MHz clock would not be sufficient and that it could produce non-linearities in the frequency chirp. If the total number of steps is  $N$  to describe a linear sweep of  $f_{ch}$  over the time  $T$  then the frequency separation between steps is  $\Delta f = f_{ch}/N$  and the FWHM of one frequency step (small pulse) would be  $f_{FWHM} = 2/(T/N)$ . In order to get smooth line we demand that the Fourier width of the small frequency steps overlap, that is that the separation in frequency is smaller than the width,  $\Delta f < f_{FWHM}$ . Putting in the variables we arrive at:

$$N > \sqrt{\frac{T \cdot f_{ch}}{2}} \approx 11,$$

where typical experimental values have been inserted,  $T = 5 \mu\text{s}$ ,  $f_{ch} = 50 \text{ MHz}$ . With the clock running at 40 MHz the total number of steps during the  $5 \mu\text{s}$  will be 200. We can then note that 200 is more than an order of magnitude larger than 11 so it appears as though the number of steps is quite sufficient to produce a linear chirp.

The oscilloscope used in the experiment was a Tektronix TDS 540, which has a sampling frequency of 1 GS/s. The linearity of the waveform generator itself was also checked with this oscilloscope, and no hint of the sweep being in discrete steps was found.

### 3.2 The photon echo material

The material used in these experiments is the crystal YAG (Yttrium Aluminium Garnet,  $\text{Y}_3\text{Al}_5\text{O}_{12}$ ) doped with rare earth Thulium  $\text{Tm}^{3+}$  ions. The Thulium ions replaces Yttrium  $\text{Y}^{3+}$  ions in the crystal lattice. The crystal sample is a cylindrical piece with a diameter of 6 mm and a thickness of 5 mm. The doping concentration was 0.1 %.

It is the  ${}^3\text{H}_6 \Rightarrow {}^3\text{H}_4$  transition in the Thulium ion that is of interest. This transition has a centre wavelength of about 793.16 nm. The coherence time  $T_2$  of the excited state  ${}^3\text{H}_4$  is about  $25 \mu\text{s}$  at 3.5 K, which is close to the working temperature in these experiments. This can be extended to over  $100 \mu\text{s}$  at even lower temperatures and if a magnetic field is applied to keep the spins of the surrounding ions from flipping randomly, thus causing disturbance. The lifetime for the excited state is around  $800 \mu\text{s}$ . The excited ions can also decay to the metastable state,  ${}^3\text{F}_4$ , which has a lifetime of about 10 ms.

This material was chosen because it has a wavelength where diode lasers are readily available. It also has a long excited state coherence time, something several similar crystals doped with rare earth ions have. This is because the transitions that are investigated occur within the 4f shell and the 4f orbitals are shielded from the disturbing environment by 6s electrons. Yet another good property is that Tm ions have a nuclear spin of  $I = \frac{1}{2}$ . This means that there are no hyperfine splittings that causes difficulties if there is no magnetic field applied.

A goal of this master's thesis is to compare equipment and experimental performance with several other experiments. As the Tm:YAG was used in all of those other experiments, this material was also needed here to better compare the results.

### 3.3 Experimental set-ups

Two main experiments were conducted, pulse compression and data storage. The set-ups are similar in many ways but different in some so two separate schematics has been included so that they can be easily followed.

### 3.3.1 Pulse compression

Here below is a schematic of the set-up for the pulse compression experiment:

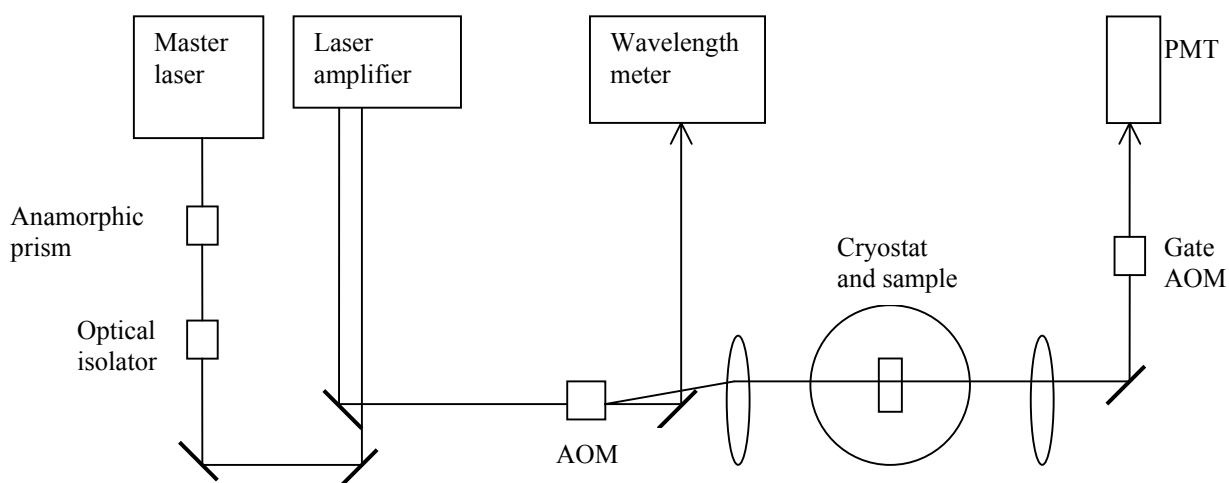


*Figure 3.3 Set-up for the pulse compression experiment. Lenses to focus the beam before and after the AOM's have not been explicitly drawn.*

Various photo diodes were used during the alignment and early measurement, but the main detection was made with a EMI 9816QB Photo Multiplier Tube (PMT) connected to the oscilloscope mentioned above.

The cryostat was a bath cryostat. The sample crystal was immersed in liquid helium and cooled down to about 4 K. To keep the helium liquid the cryostat then has several shells containing vacuum and one filled with liquid nitrogen. There are glass windows in every shell that the incoming light has to pass when it goes through the sample and out again. None of these windows were anti-reflection coated so there is a certain loss of intensity of the light in this process. These four windows as well as lenses before and after the cryostat give ten glass air/vacuum surfaces and two glass helium surfaces. The helium has a refractive index of about  $n_{He} = 1.408$ , which is close to the glass of  $n_{glas} = 1.5$  and gives no substantial contribution. The sample with a refractive index of approximately  $n_{YAG} = 1.82$ , which produces two surfaces with the surrounding helium for a loss of about 1.6 % each. The total loss from surfaces then amounts to about 35 % of the light, where dirt and imperfections have not been taken into account.

### 3.3.2 Data storage

The data storage set-up is presented below in figure 3.4. Just as before various photo diodes were used in the alignment process, which was significantly more difficult now since the two beams coming from opposite sides had to be made to overlap in the cryostat. For the main detection another PMT was used than in the pulse compression experiments. The new one was a Hamamatsu R943-02 and it replaced the other one as it was found to have better efficiency at our specific wavelength.

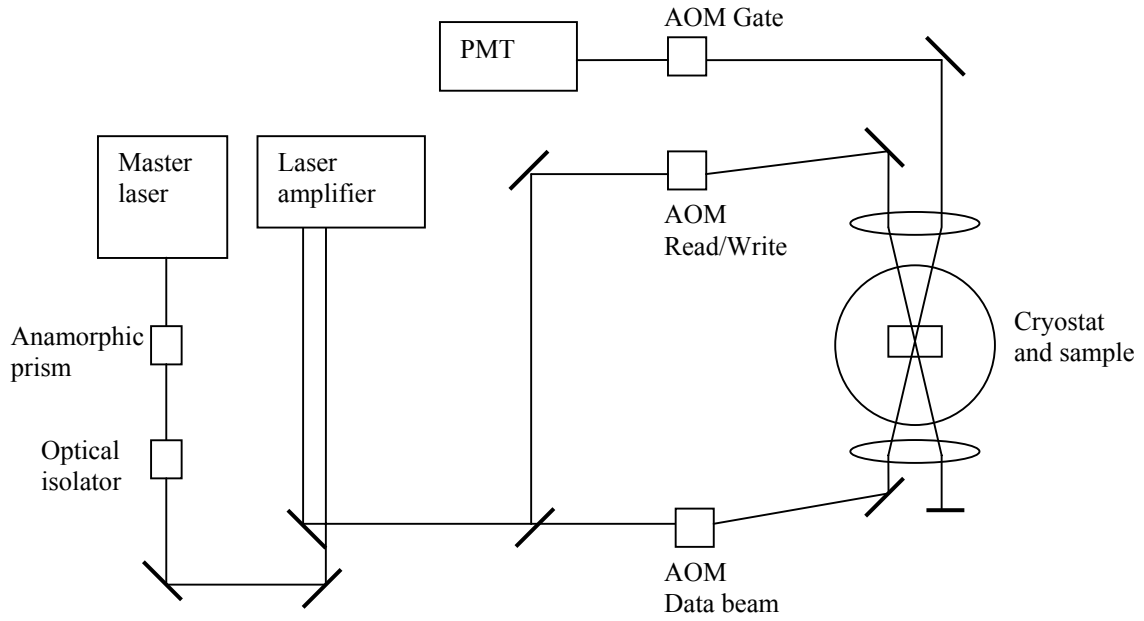


*Figure 3.4 The set-up for the data storage experiments.*

As the data storage experiments were made in another lab the cryostat was also another one (Cryovac) but it functioned in the same way. One difference though was an extra pair of glass windows in the cryostat that the beam had to pass through, which further increased the losses in the surfaces somewhat.

## 4. Results and discussion

### 4.1 Optimisation of the amplifier

The first thing to test was how well the amplifier worked. There was a need to know how much power it could yield while still keeping the ASE to a minimum. A way to measure this is by looking at the spectrum from the beam coming out from the amplifier. As figure 4.1 below shows there were two main peaks, the light coherent with the master laser at 793 nm and then the spontaneous emission from the amplifier at a higher wavelength above 800 nm. The objective was to minimise the ASE peak, while maximising the output power.

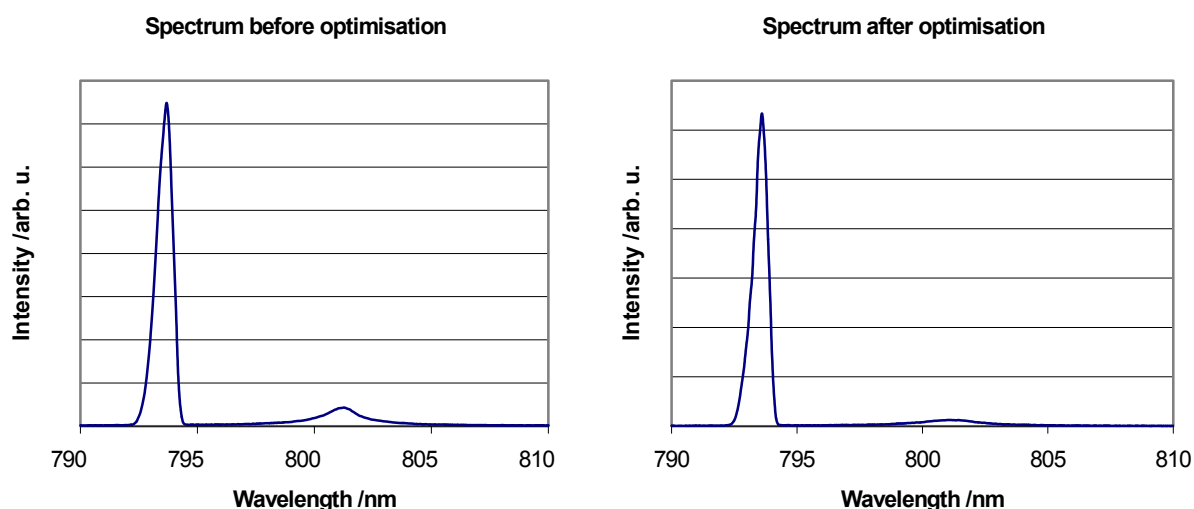


*Figure 4.1 The spectrum of the beam after the amplifier. The small peak to the right around 801 nm in both pictures is the ASE, which is relatively small compared to the injected beam at 793 nm after the amplification.*

The diagram to the left shows how the spectrum looked like before the optimisation began and the one to the right shows the spectrum after many hours of tweaking on the lens system in the amplifier. One can see that the ASE is almost gone completely in the right part of figure 4.1. To quantify this, it can be said that the ASE peak in the graph before optimisation was about 6 % of the injected peak, while the relative size of the ASE peak after optimisation was about 2 %. As the ASE was diminished the power of the outgoing beam was increased from 90 mW in the beginning up to 125 mW after optimisation, so it is fair to say that the objectives regarding the optimisation were reached.

After the beam was proven to have the right qualities, the next step was to create a general two-pulse echo, and to optimise the signal of that echo. This could be done by moving the lenses next to the cryostat for better focus and by checking that the AOM's and PMT were working well enough to distinguish the echo from the background noise. As mentioned in the previous chapter, photo diodes were used for detection during alignment. These are much easier to use than the photo multipliers, but are slower and thus have much longer rise and fall times. This would make the limits for the width of the echo to about 100 ns, which is much longer than the compressed echoes were expected to be later on. The limit on the PMT is instead around 4 ns, so it is much more suited for our pulse compression experiments.

## 4.2 Pulse compression

In all the measurements on pulse compression the time between the two pulses in the photon echo process was chosen to be  $T = 10 \mu\text{s}$ . The power of the laser beam going in to the cryostat was about 45 mW, unless another value is stated for a specific experimental type. From the beam coming out of the amplifier, there was much loss of power. The main losses comes from the pulse producing AOM, where about 50 % was lost, but other sources of loss are imperfections in the mirrors and reflections from the lenses. It should also be noted that talking about compressed pulse durations means the FWHM of the echo, while the incoming pulse duration means the duration of the first pulse. The second pulse in the compression process has a duration that is half of the first pulse.

### 4.2.1 Constant chirp rate

The first series of measurements were performed while holding the chirp speed constant. This means that as the duration of the ingoing pulse was increased from shot to shot so was the total frequency interval used in the chirp. The two pictures below show echoes from these measurements with different values on the pulse duration,  $T_d$ , and chirp interval,  $f_{ch}$ .

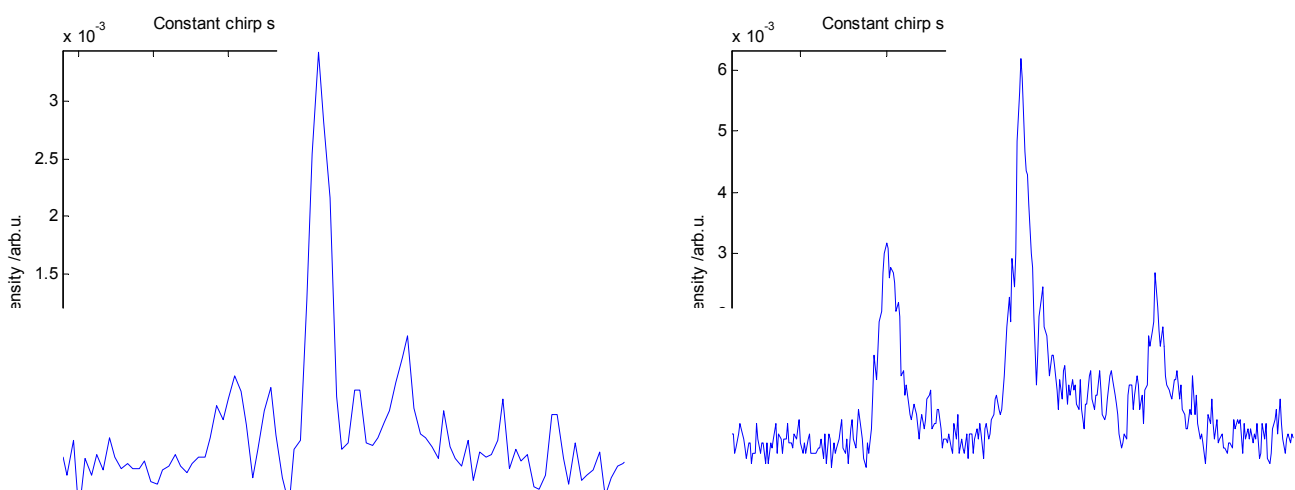


*Figure 4.2 These figures show a compressed echo using a constant chirp rate. The one to the left has a lower chirp range and the one to the right a higher as can be seen from the numbers. Note that the scales on the axes are not the same in both cases. The one to the right was also done using a higher number of measuring points which gives a higher resolution.*

The widths of the two compressed echoes shown in figure 4.2 were measured to be 32 ns and 17 ns respectively. Besides the echoes shown, which were done with 3 and 8  $\mu\text{s}$  long pulses, measurements were also done on an intermeditate pulse duration, namely 6  $\mu\text{s}$ . Several shots were made on each setting and a comparison between the average values and the theoretical limitations, given by equation (8) in chapter 2, are presented below in table 4.1.

Frequency range $f_{ch}/\text{MHz}$	Theoretical FWHM $0.88/f_{ch}/\text{ns}$	Experimental FWHM $T_e/\text{ns}$
34	26	31
68	13	24
91	10	17

Table 4.1 A comparison between experimental and theoretical results of the duration of the compressed echoes.

All the measured values of the compressed echo durations in table 4.1 are within a factor of two compared to the theoretical limitations. In comparison with previous experiments done here in Lund this is a significant improvement. In Wangs experiments [9, 4] the compressed echoes are about a factor of 6 longer than the theoretical values at the given bandwidth of the chirp. The bandwidths used in Wangs experiments was from 23 MHz up to 230 MHz, i.e. about the same as here.

Another interesting thing that can be seen in the examples of measurement above, especially in the right part of figure 4.2, is the presence of sideband structure. There is a strong central echo, which is the one the width was measured on, and then one additional echo can be seen on each side. This structure was investigated in further detail in following experiments.

#### 4.2.2 Constant pulse duration

To separate the effect of the two parameters incoming pulse duration and chirp bandwidth, the next step was to keep the duration of the incoming pulse constant and to vary only the chirp bandwidth. A pulse duration of  $T_d = 3 \mu\text{s}$  was chosen and measurements at seven different frequency bandwidths were done. The result is presented in the graph below, where the echo durations from the experiments are compared to the theoretical values.

As can be seen in figure 4.3, at some bandwidths the experimental values are really close to the theoretical, but for higher and lower bandwidths, they diverge more. The experimental curve even seem to be going upwards at higher bandwidths. The reasons for less good results might not be the same for the lower part as for the higher part. For example, in the lower region the chirp interval is only about 5 MHz. Any fluctuations in the laser, AOM drivers or anything else that can cause a change in frequency, will effect the lower region the most. Drifts in frequency between the two pulses in the echo process will diminish the

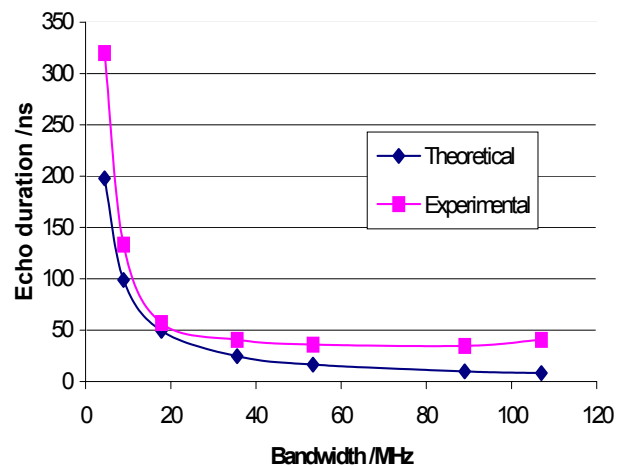


Figure 4.3 The duration of the compressed echo as a function of the bandwidth used in the chirp. Both experimental and theoretical values are given for comparison.

frequency overlap, which reduces the effective bandwidth, and thereby increasing the compressed echo duration. Still, in the lower bandwidth region the experimentally measured duration is within a factor of two compared with the theoretical.

On the other hand, the measurements made with large bandwidth should be fairly forgiving to small drifts in frequency somewhere. However, the intensity decreased significantly for the echoes made with larger bandwidth, which made measurements of the duration more difficult, as noise had a bigger impact. One reason for the decrease in intensity is probably that the duration of the incoming pulse was too short to make effective use of the large frequency range. The larger the frequency interval the more atoms get involved in the process. And as the total incoming power is the same this means that the intensity on atoms in a certain frequency range will be less the higher bandwidth is used. The pulse area, described by equation (4) in the theory section, might then be decreased to something less than the optimal  $\pi/2$  pulse.

A large contribution to the noise in these experiments, were bubbles in the liquid helium. Partly micro bubbles, which blurs the laser beam to a more diffuse spot. This effect was ever present and generally decreased the intensity of all the shots equally much. The other part was larger bubbles, which only comes into effect on some of the shots. These bubbles move on a much slower time scale than the course of the echo process. Therefore, the way through the cryostat might be clear of bigger bubbles sometimes, giving a strong signal, and obstructed by a bubble sometimes, which takes away almost the whole signal by scattering in that bubble.

Here below figure 4.4 shows an example of an echo, measured both as a single shot and by letting the oscilloscope average over 20 shots.

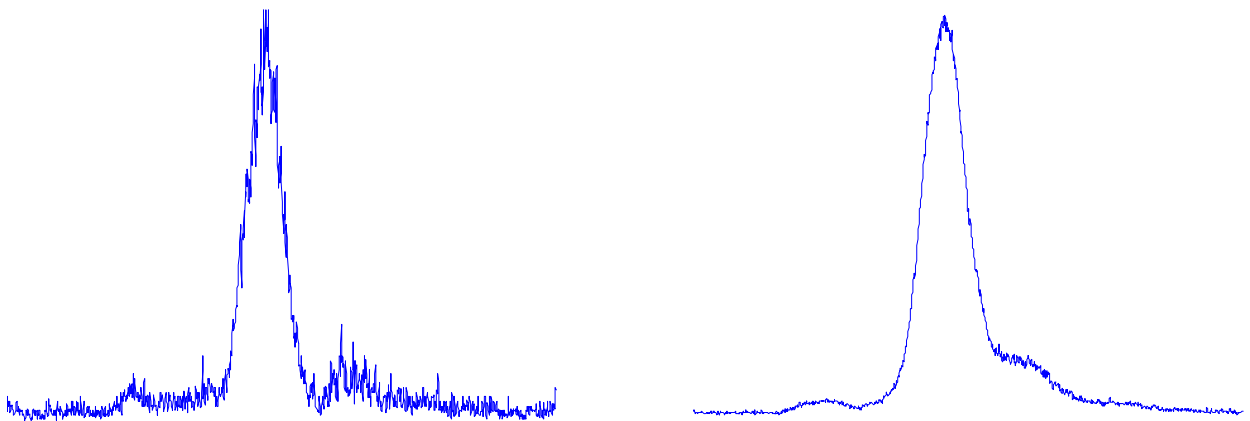


*Figure 4.4 Comparison between a single shot measurement and an average over 20 shots. Both left and right part at the same settings otherwise.*

Apart from the obvious fact in figure 4.4 that the average is a smoother curve due to much less random noise, there are a couple of interesting things to note. It might be hard to see in the figure above but zooming in and measuring the FWHM, the results would be that the width of the single shot peak is around 320 ns, while the width of the average peak is around 410 ns. Average measurements were made on all the different bandwidths presented in figure 4.3, and the same broadening could be seen in all. The reason for this is that the

single shot peaks jitters a bit back and forth from shot to shot. This is believed to be an effect from the laser, that for example drifts in frequency between the first and the second pulse are different from shot to shot.

Even in the right part of figure 4.4, where the average is displayed, some of the side band structure mentioned earlier can be seen. It is also interesting to note that it appears to be slightly asymmetric. According to the theory, the shape of the echo should be a sinc function, which indeed has some small side peaks. They are, however, neither as large as seen in figure 4.2 nor asymmetrical as seen in figure 4.4, so just looking at these figures it seemed as though there was some other effect involved also.

### 4.2.3 Adding deformations to the chirp

In an attempt to understand where the deformations of the echo shapes shown above come from, the previous experiments done here in Lund on the subject were examined. In particular Afzelius Master's Thesis [4], which handles analytical as well as simulated models of how the photon echo process works. There it is found that a quadratic term to the frequency chirp, as described briefly in the theory chapter, can give such asymmetric side bands.

Knowing this, a logical next step would be to add a quadratic structure to the supposedly linear chirp and see how the echo behaves. If it indeed were this error, it would perhaps be possible to correct the shape by adding a counteracting quadratic term to the chirp.

In figure 4.5, a series of pictures showing the echo shapes for different values of the constant  $L$  is presented. Here  $L$  is the constant in equation (9) that determines the strength of the quadratic term. Note that the values given are those used internally in the waveform generator and are useful for comparison. They are not given in any physical units, but can be transformed to that linearly. The calculated limit where these effects should begin to show according to theory, is  $|L_{limit}| = 1.44$  in my units. This would correspond to a physical value of  $L = 2 \cdot 10^{10}$  Mrad/s<sup>3</sup>. Around  $L_{limit}$  not too much of the effect can be seen, but for a bit higher values of  $L$ , clear asymmetrical side bands can be seen. For positive values the side bands occur on the right side of the central peak and for negative values on the left side. Besides the clearly visible peaks that arise from the quadratic term, there are a couple of smaller side peaks in all six of the pictures, even in the ones where  $L$  is close to or below the limit. As they don't change with  $L$ , these are probably not an effect from a quadratic shape of the chirp, furthermore the size and placement of those are fairly matching with the ones seen in e.g. figure 4.4. This means that while the quadratic effect theoretically arrived at has been checked experimentally to be true, the structure of our experiments has yet to be explained.

Another deformation in the chirp the echo is supposed to be sensitive to, again according to the theories in [4], is if the chirps in the two incoming pulses are not swept over the exact same range. It was predicted that a change of only 0.5 % larger interval in the second chirp would result in a broadening of the echo by a factor of 22, combined with a loss of intensity. This was investigated, and a small effect was seen, but not anything near the predictions. The second chirp range was varied as much as 20 % up and down, but the width of the echo didn't increase more than a factor of 2. Exactly where the difference between theory and experiment comes from is uncertain, but it should be noted that the calculations were based on a bandwidth of 500 MHz, where as only up to 35 MHz was

used in the experiments. This might play a role as the echo in the calculations would be compressed a factor of 5000, while the echoes in this experiment were only compressed a factor of about 20. It is not impossible to imagine that such a high compression is much more sensitive to various errors.

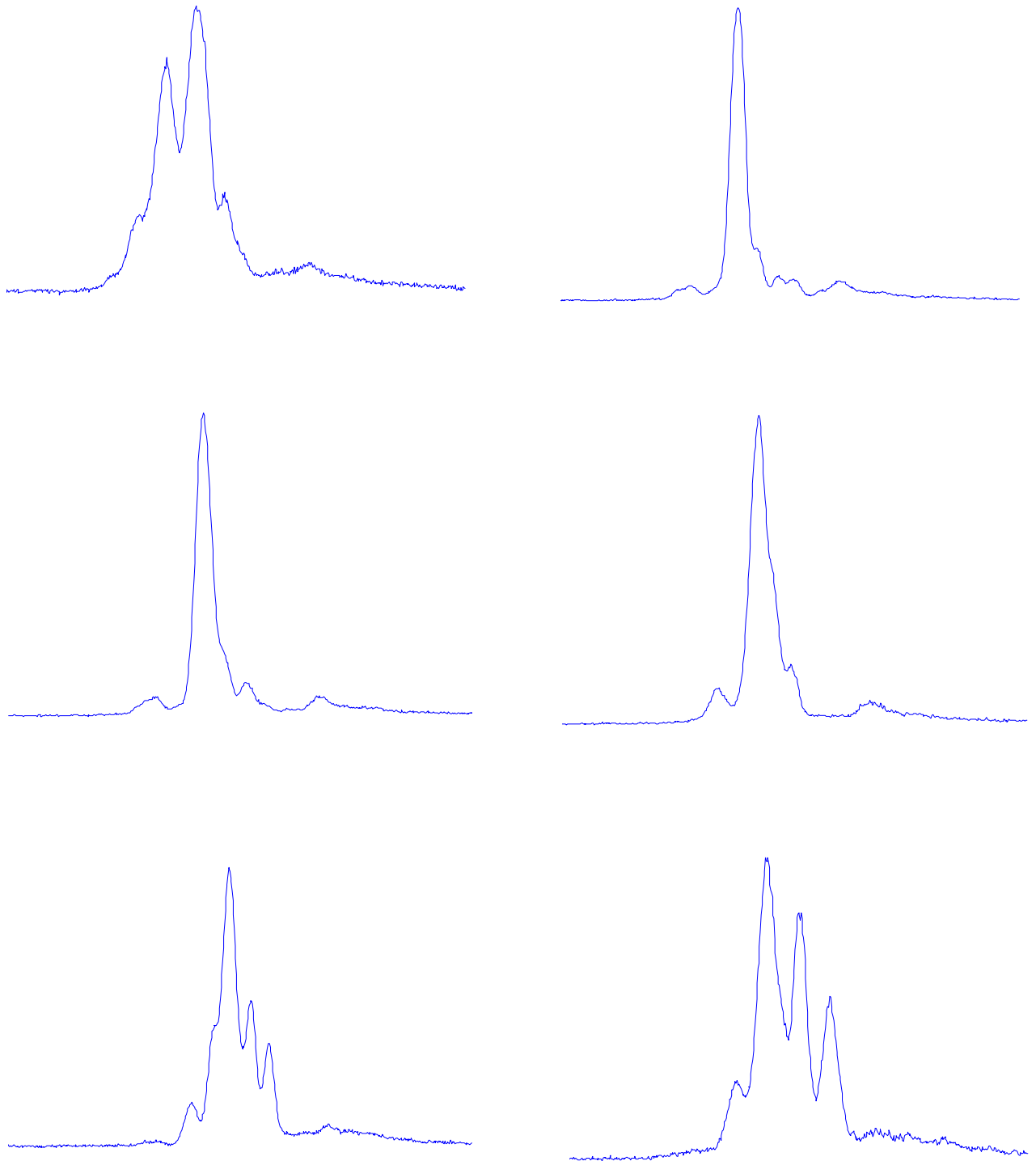


*Figure 4.5 Six pictures showing different echo shapes depending on how strong the quadratic term was made. Values  $L = -5, 0, 1, 2, 5$  and  $9$  were chosen, where  $L = 0$  means that the chirp is the supposedly linear chirp as used before and where  $L = 1.44$  is the limit where the distortions of the signal should start to show.*

#### 4.2.4 Laser power dependence

Another goal of this thesis was to check the effects of the higher power used here compared to previous experiments. In [10] it is said that the output power of the laser in Wang's experiment is about 30 mW, which with 2 AOM's in series would correspond to a power of about 6-7 mW after the AOM's but before the cryostat. It is also in this position that the values of the beam power is given for these experiments presented in figure 4.6. There are then additional losses in lenses and in the windows of the cryostat as mentioned in the previous chapter, but those losses should be the same in both Wang's and in this experiment. The four pictures given in figure 4.6 show single shot measurements of a compressed echo for three different input powers. The first three at the same chirp bandwidth and incoming pulse duration, and the last one with much longer pulses and higher bandwidths were used.

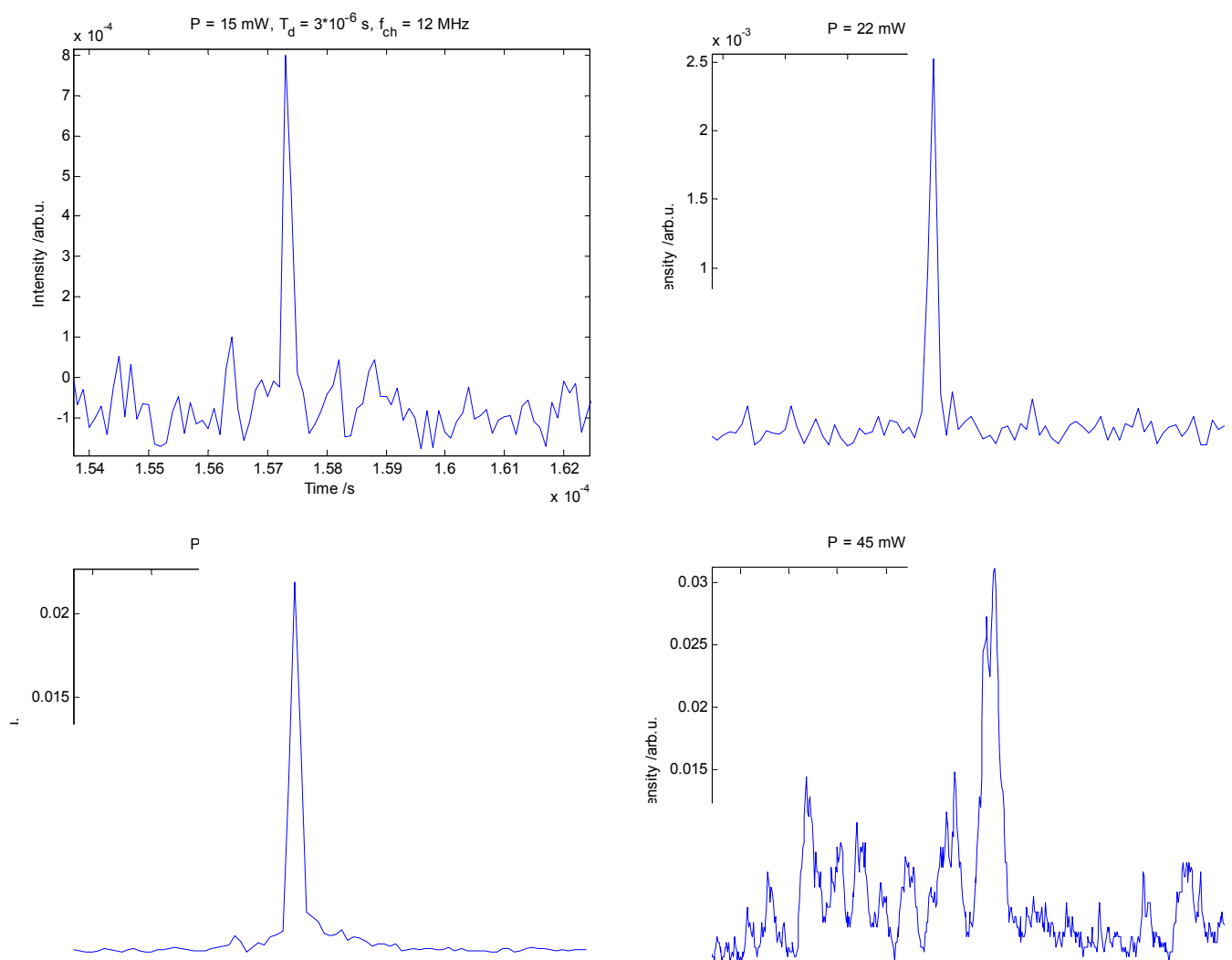


Figure 4.6 Comparison between single shot measurements of different beam powers. The last picture shows a situation where a much longer incoming pulse was used. Note that the scale on the x-axis is not the same for the last picture.

The three first pictures in figure 4.6 above, show exactly what the theory describes, i.e. the intensity of the echo increases with the intensity of the incoming beam. Reading the value of the intensity on the peak in the three different cases, one can see that it is about  $8 \cdot 10^{-4}$  (arbitrary units) in the first case where the beam power is 15 mW. In the 22 mW case the intensity is about  $25 \cdot 10^{-4}$  giving a ratio between the two of approximately 3.1. In the theory section it is mentioned that photon echoes are a third order process, which means that the intensity scales as  $\sim I^3$ . So the theoretical ratio between the first two cases would be  $\left(\frac{22}{15}\right)^3 \approx 3.2$ , in very good agreement with the experimental results. Doing the same calculations between the 22 mW case and the 45 mW case, we get a theoretical ratio of 8.6, which again is close to the experimental at 8.8.

Practically, this increase in power can pay off as the signal will be much stronger compared to the background noise. This is also effectively seen in the three first pictures in figure 4.6, the noise is clearly visible in the 15 mW case, but almost completely gone in the 45 mW case.

Now, the last of the four pictures in figure 4.6 is also taken at 45 mW, so the background noise should be very small. This leads us to believe that the many peaks seen in this picture is something else than noise. The difference in this case is that the pulse duration is much longer, while it at the same time is scanned over a larger interval so the chirp rate is the same. Recall from the description of the laser in the previous chapter that its linewidth is about  $\Gamma_{laser} = 300$  kHz. This gives us that the coherence time is in the order of  $\tau = 1/\Gamma_{laser} \approx 3 \mu\text{s}$ , which is also the order of the duration of the incoming pulses. Therefore an increase from pulses with a duration of  $3 \mu\text{s}$  to pulses with a duration of  $9 \mu\text{s}$  will increase the effects of drifts in laser frequency significantly. Such drifts could be seen as a sudden and random change in the phase of the laser field. Imagine for example that the laser makes one relatively large phase shift during one of the pulses. There will then basically be two echoes created, appearing at the same time, but with different frequency components and with different phases. These phases will counteract each other at some times and interfere constructively at other times, as the phase velocity is different due to the echoes being made up from different frequency ranges. Figure 4.7 below demonstrates how the echo can be build up in two different cases. One is a perfect echo, for reference, when there is no phase jump in the laser. The other picture shows how the echo may change when the phase of the laser begins to drift continuously after a part of one of the pulses. Comparing the right picture in figure 4.7 with the last in figure 4.6 some similarities can be seen. Mainly a strong central echo surrounded by periodic smaller peaks. Upon closer inspection the simulated picture even seem to display some asymmetrical properties also found in the experimental picture.

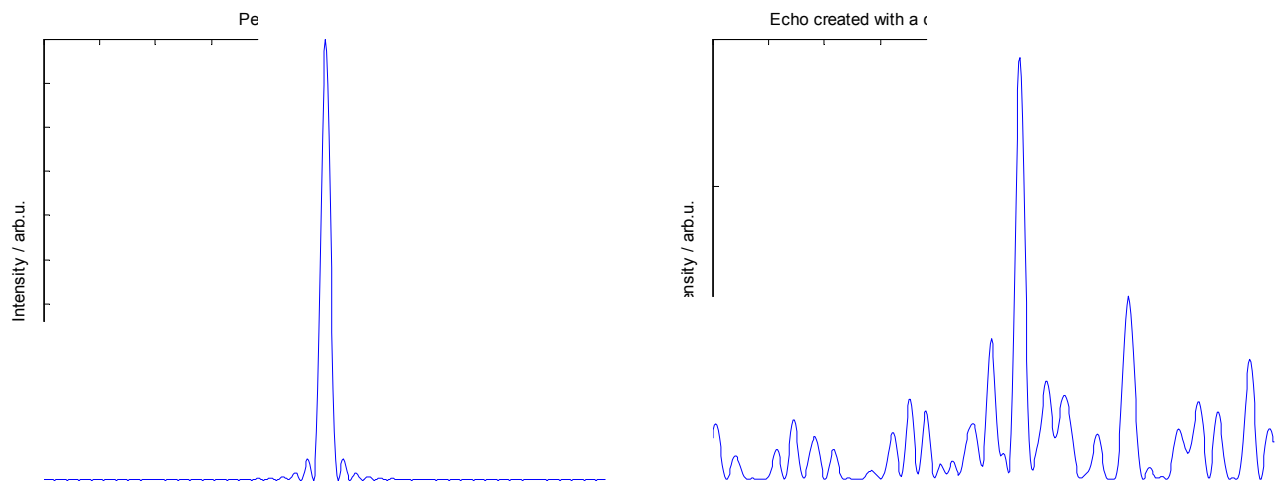


Figure 4.7 The left part shows a perfectly created echo, whereas the right part shows an echo created with a (cubic) continuous drift in the phase of the laser field. The drift was set to start some time into the chirp.

Before all the experimental data had been analysed we believed that some of the echo deformations came from what is called excitation induced frequency shifts. Typical instances where this effect can occur is when the pulses are long and the chirp bandwidth large. This creates complications in the material as keeping the beam on for a long duration means that many of the ions in a frequency range will be excited, and also making the bandwidth larger means many excited ions over a large interval. If too many ions are excited they will begin to disturb the surrounding ions and shift their frequency, as their dipole moments are coupled. Many different shifts in frequency will occur, depending on how they are placed in respect to each other, and the result would be a smearing of the echo. More details of what happens can be found in e.g. [11] where this phenomenon has been measured for the Tm:YAG crystal used in these experiments, or in [12] where a more theoretical investigation is made. In [11] it is found that for a crystal such as the one used in these experiments a broadening of the echo would be about 120 kHz per MHz interval of fully excited ions.

#### 4.2.5 High compression echoes

As a final experiment on pulse compression, the knowledge gained about the parameters of the echo was used to get as high compression as possible for a pulse. Even though it may seem from the evaluation of phase shifts in the laser above that an optimal echo would require pulses of shorter duration, this was not entirely true. Experiments where a short pulse duration was used combined with a large bandwidth, generally yielded very bad echoes, in the meaning that the surrounding structure was of the same intensity as the central echo, in those cases where a central peak could be found at all. The reason why shorter pulses did not give good results has not yet been found, though some part of the problem could be the equipment. If one uses larger ranges of frequencies while doing the pulses shorter, the net effect would be a much faster chirp. This shouldn't be a problem in theory, but practically performance in e.g. electronical devices may be reduced and may thus cause errors.

So, an incoming pulse with a duration of 9  $\mu$ s was chosen, and figure 4.8 displays an example of one of the shortest echoes produced.

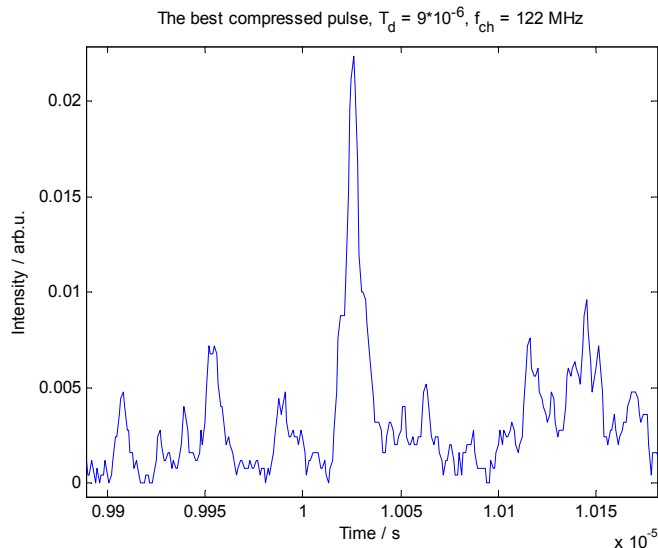


*Figure 4.8 One of the shortest and most compressed echoes done during these experiments.*

The pulse in figure 4.8 has a FWHM of around 7.5 ns, which is very short compared with the original duration of 9  $\mu$ s. The pulse would in essence have been compressed a factor of 1200, which is a lot more than the previous experiments done here in Lund where they got a compression factor of about 450 [9] using the same technique. It is also not very far away from the theoretical limit, which at this bandwidth is about 7.24 ns.

## 4.3 Data storage

As described in the theory section for swept carrier time domain data storage, what governs the time  $T$  between the first pulse, write beam, and the second pulse, data beam, is determined by the frequency shift between the beams at the selected chirp rate. This shift is produced by changing the driving voltage to one of the AOM's. To get a good view of how the frequency of the AOM's vary with applied voltage, this was measured by simply connecting the radio frequency output on the AOM driver into the oscilloscope and there do a fast Fourier transform. The laser frequency after an AOM will simply be the AOM frequency added to the frequency of the incoming laser beam. A table for each AOM was created for use later in the experiments. It was found that the gradients for the AOM's was about 3.5 MHz/V and the shifts used during the experiments were typically in the order of 2 – 3 MHz.

### 4.3.1 General parameters

The first experiments on optical data storage was to investigate how this process would behave when some general parameters were varied. These parameters were bit length,  $t_b$ , the time distance between bits,  $\Delta t_b$ , and the time between the write beam and the read out beam,  $t_{wr}$ . Figure 4.9 below shows data storage where  $t_b$  was varied, to the left, and where  $\Delta t_b$  was varied, to the right. The 10 bits shown in the picture to the left, are all of different bit lengths, starting from 100 ns in the leftmost bit and going up to 1  $\mu$ s in 100 ns increments. The sequence of bits to the left in this picture displays the part of the data beam that goes through the closed gate AOM, while the sequence to the right is the actual signal

from the echo. The plateau where the echo signal is, comes from light going through the AOM that pulses the data beam.

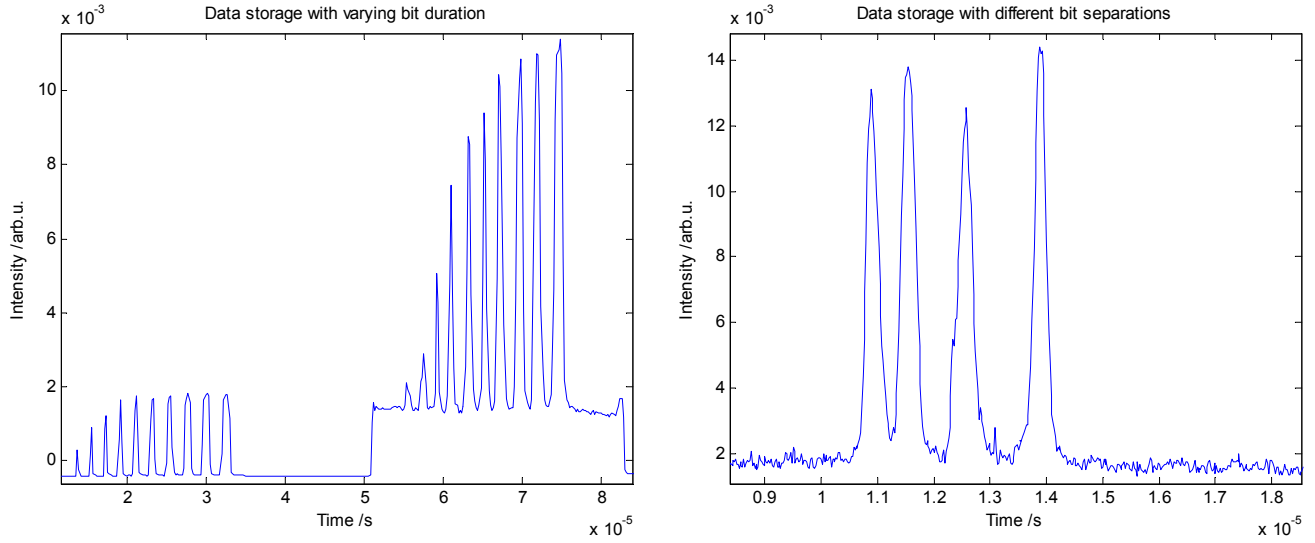
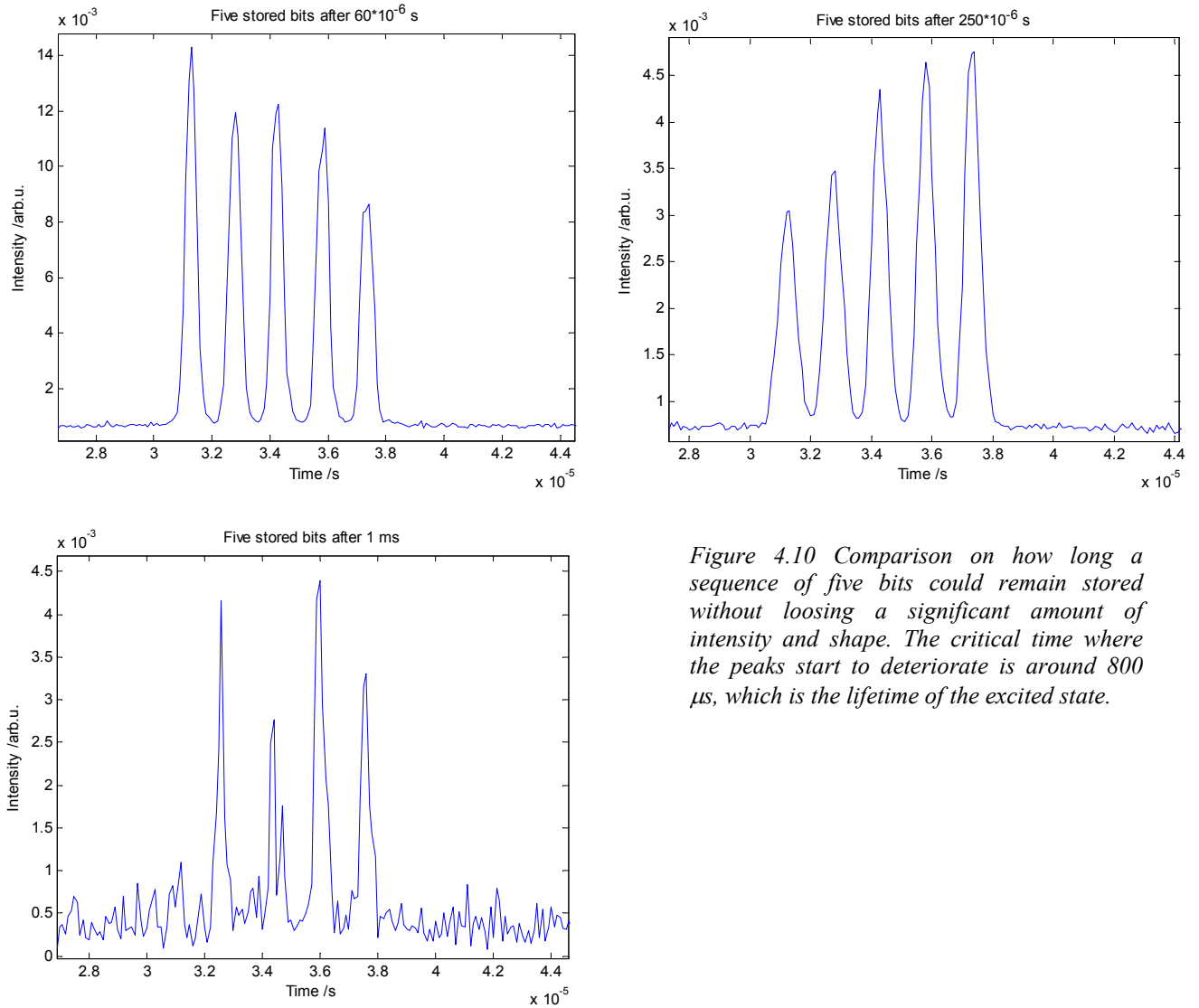


Figure 4.9 Shows bits with varied bit duration, to the left, and with different time separation, to the right. See the text for further information. The picture to the left also shows how the data beam can be detected through the closed gate.

In the left part of figure 4.9, it can be seen that the echo signal is much lower for the short bits around 100 – 200 ns and looking at the data beam signal through the closed gate, the same thing can be seen. This implies that such short bits are not a problem in the photon echo process, but rather some technical issue. The best explanation seems to be that the data AOM starts to end the pulse before it is at its maximum as the rise time for the AOM is in the same order as 100 ns, as mentioned in section 3.1.3. Therefore, in the further experiments a bit duration of at least 300 – 400 ns was chosen. Note that it would also have been possible to improve the rise time by focusing the laser beam harder into the AOM. A more narrow focus means that the acoustic wave need less time to interact with it, which gives a shorter rise time.

The right picture shows the time separations 700 ns, 1  $\mu$ s and 1.3  $\mu$ s. This test was done to see how close it would be possible to have the bits. While there is a good separation in time between the last bits, the two first bits have begun to merge, so generally the separation between bits were kept at more than 700 ns.

The measurements on data storage where the time between write and read was changed were done at three different time separations. First after 60  $\mu$ s, which is a short time not long after the readout pulse has ended, and then in other shots with  $t_{wr} = 250 \mu$ s. This is a longer time but still significantly lower than the lifetime of the excited state at 800  $\mu$ s, so we would expect the echo signal to still be fairly strong. The last measurements were done with separations between write and read pulse of about 1 ms. As this is longer than the lifetime of the excited state we would now expect to see a drop in intensity. Figure 4.10 below show pictures of a stored bit sequence of five bits recalled after the three time intervals mentioned. The first two pictures were taken at the same settings so they are comparable when it comes to the scale on the intensity axis, but in the last picture the amplification on the photo multiplier tube was increased, as the signal was much weaker. This can be seen on the higher noise levels around the main peaks.



*Figure 4.10 Comparison on how long a sequence of five bits could remain stored without losing a significant amount of intensity and shape. The critical time where the peaks start to deteriorate is around  $800 \mu\text{s}$ , which is the lifetime of the excited state.*

Figure 4.10 clearly shows how the shape of the bit sequence gets worse as more of the population in the excited state gets deexcited. As only a fraction of the ions decays to the metastable state, which has a longer lifetime of about 10 ms, it is clear that the intensity should drop visibly, but it does not explain the bad echo shape, where not even all five bits could be identified clearly. Note that the last picture in figure 4.10 is only one example of the results from the 10 ms experiments. The other results looked similar but there was no symmetry to be found, i.e. it was not possible to say that it was always bit two and three that had the worse shape for example.

The parameters used in the sequence above were a bit length of  $t_b = 450 \text{ ns}$  and a bit separation of  $\Delta t_b = 1.5 \mu\text{s}$ . The frequency offset between the beams was  $f_{\text{off}} = 2.5 \text{ MHz}$  and the chirp rate was about  $2.5 \text{ MHz}/\mu\text{s}$  so the time between the write beam and the data beam would be  $1 \mu\text{s}$ .

### 4.3.2 Comparison to previous work

The next series of measurements was done in purpose of comparing these experiments with those done in Nilsson's master's thesis [13], where the chirp rate was varied for constant bit lengths. The exact same values on bit length, time separation between bits and the different

chirp rates as in Nilsson's thesis were used. Two different series of experiments were made, either with a bit duration of 500 ns or with 100 ns. In both series the time separation between bits was  $\Delta t_b = 2 \mu\text{s}$  and the chirp rate was varied from 1.7 MHz/ $\mu\text{s}$  down to about 1.1 MHz/ $\mu\text{s}$ . A bit duration of  $t_b = 100 \text{ ns}$  was used in Nilsson's thesis and so it was also used here, even though as we have seen the slow rise time of the AOM made the intensity of such short pulses much lower. Figure 4.11 below presents the results from these measurements using the fastest and the slowest chirp rates for each of the two experimental series.

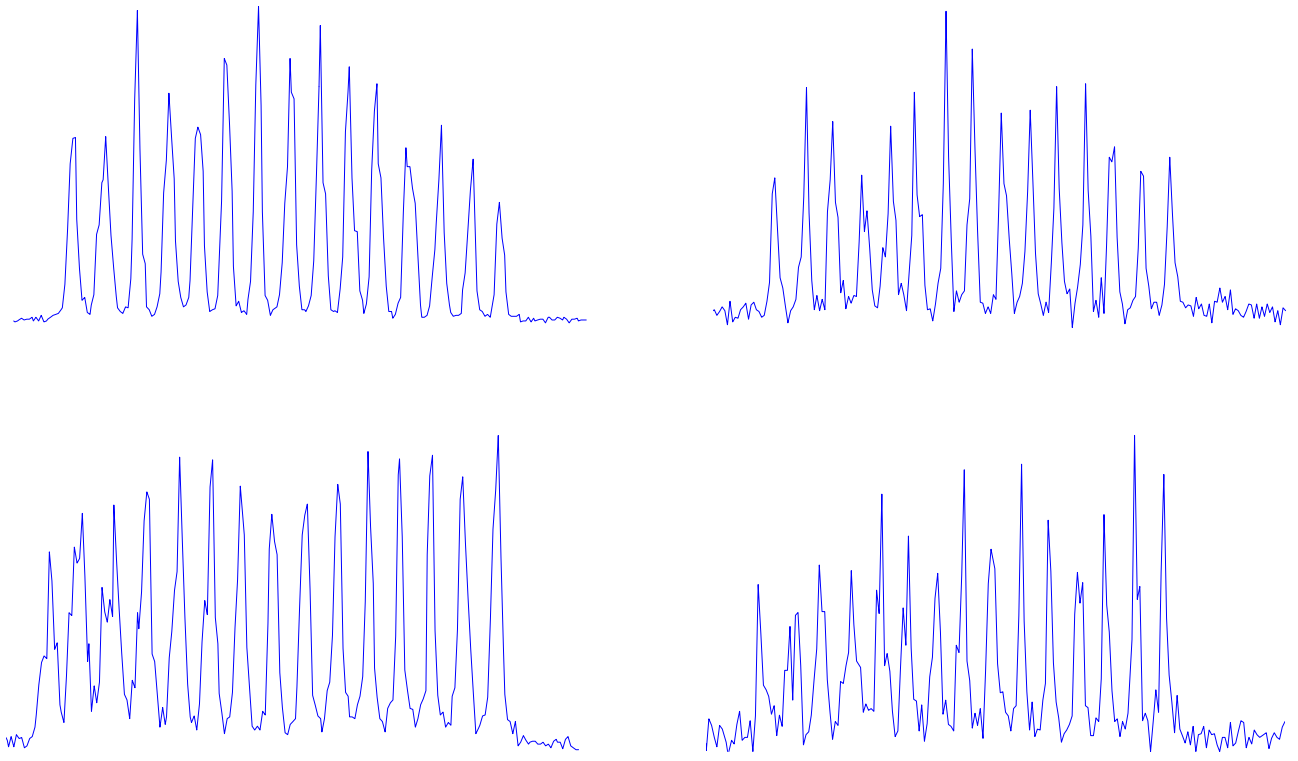
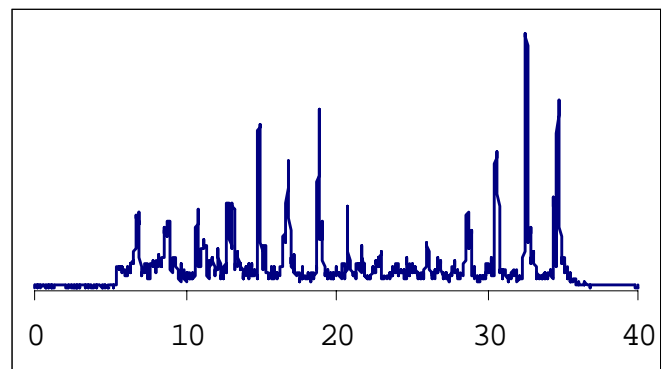


*Figure 4.11 Different chirp rates were tested for bit sequences with bit lengths of both 500 ns and 100 ns. The data to the pictures on the right, where the bit length is only 100 ns, were taken with a higher amplification on the PMT. The last picture is taken from Nilsson's thesis [11] and displays the recalled sequence at a chirp rate of 1.1 MHz/ $\mu\text{s}$  and bit length of 100 ns.*



In the original experiment in [13], it was expected that the shapes of the echoes would be considerably worse when the chirp rate was only 1.1 MHz/ $\mu\text{s}$  as it is in the two lower pictures in figure 4.11, and this was also shown. This is because of the linewidth of the laser. It was around 400 kHz, which is about the same as the linewidth for the laser in these experiments, i.e. about 300 kHz. This means a coherence time of about 3  $\mu\text{s}$  as mentioned

in the previous chapter. Given a bit length of 500 ns, the frequency width of the bits will be around 4 MHz, which then sets a value on the chirp rate needed to cover this frequency range within the coherence time. This limit will be around 1.3 MHz/ $\mu$ s. The corresponding limit for Nilsson's experiments would then be 1.6 MHz/ $\mu$ s, so in both instances for the 500 ns bits, the upper picture is above this limit value, while the lower is below it. This effect was seen clearly in Nilsson's experiments but not at all in these experiments. Even harder restrictions arise when the bit length is only 100 ns, as in the pictures to the right. These bits would span a 20 MHz interval, which would require a chirp rate of about 6.7 MHz/ $\mu$ s, about a factor of 4 more than what was used here. Still the shapes of the echoes were deformed very little, only showing slight irregularities in the top of some of the peaks. This leads us to believe that the laser may have been more stable in this experiment than the stated 300 kHz.

Another interesting thing to note about using as slow chirps as here, is that the bits are not stored in separate frequency channels, but instead they overlap. Even for the highest chirp rate 1.7 MHz/ $\mu$ s, the scan will only cover about 3.4 MHz in the 2  $\mu$ s between the bits. This is not enough to cover the 4 MHz of the 500 ns bits, let alone the 20 MHz for the shorter bits. So, despite all bits overlapping in frequency the recalled bit sequence is of very good shape also indicating good laser stability.

### 4.3.3 Final test on data storage

As a conclusion to data storage a couple of experiments were made with the goal to simply store many bits of data. This didn't quite work out. Most of the bits were read out in good shape but bits on certain periodic intervals disappeared completely, or were in a very bad quality. This can be seen in figure 4.12 below, which shows the typical storage of a 60-bit sequence.

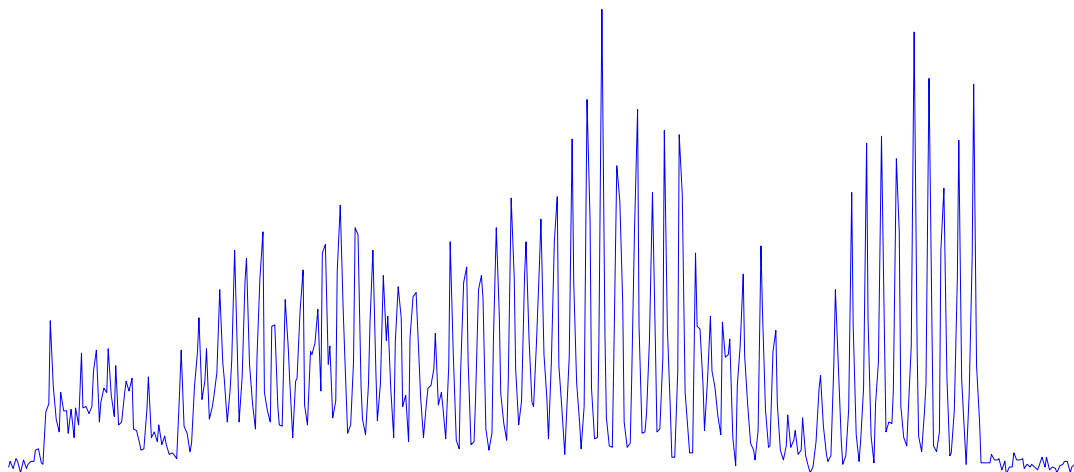


*Figure 4.12 A recalled 60-bit sequence consisting only of ones. Much deteriorated echoes in the beginning as well as a clearly noticeable absence of echoes at about 115  $\mu$ s.*

Not much more of this behaviour will be said. Due to a scheduled renovation of the laboratory there was never time to find the reasons for these errors.

## 5. Conclusion

Most of the experimental time was concentrated on the pulse compression experiments. There were several issues in this area brought up in different previous experiments here in Lund [4, 9]. For example there were experimental deviations from the theoretically possible echo widths by a factor of 6, which were not completely explained by the models. It was though that these deviations could be made much smaller with the new laser system used in this thesis, and as shown in chapter 4 this was indeed possible. The errors for the FWHM of the echoes were mostly within a factor of 2. However, there arose new kinds of structures such as the discussed side peaks that had not been seen before. Comparing the results from all the different experiments it can be noted that the peaks are clearly visible in some of the pictures but not seen at all in some. This leads us to believe that it may be something random that causes these phenomena, maybe connected to the equipment for example.

In some experiments, see e.g. figure 4.7, erratic behaviour seemed to be well explained by phase shifts in the laser. In other experiments however, like the ones done on data storage (e.g. fig. 4.11), the laser seemed to be exceptionally stable compared to what was expected. It therefore seems possible that some characteristics of the laser varied over larger time scales, like days or weeks. The laser might also have been more unstable due to more uncontrollable effects such as small vibrations caused by the cryostat pumping system that was not the same in the different experiments etc.

As a main source of background noise in these experiments, bubbles in the liquid helium was mentioned. It is actually possible to compensate for this by pumping vacuum in the helium chamber. Below a certain critical pressure the helium will turn superfluid and this will effectively remove all bubbles. It was tried once, and the result was very stable echoes. The drawback was that in this cryostat the helium boiled off at a drastically increased rate, giving very little time to perform any experiments before all the helium was gone and the sample began to rise in temperature.

Overall there were many photon echo effects examined and explained in this thesis. This was also a major goal of this work in addition to testing the new equipment. The amplifier took some time to align at first, but a gain of 4 was reached almost completely without ASE, which was a successful result. Unfortunately there was little time to make a serious try at storing many bits in one spatial point, but the final results on pulse compression was good. At most a laser pulse was compressed more than a factor of 1200, which is an improvement compared to the factor 450 obtained in the previous experiments.

A suggestion for further improving experiments with photon echoes would be to try to make the laser even more stable. It would also be a significant improvement to be able to make the helium superfluid for a longer period of time, thus removing the primary source of noise. As was noted in section 4.3.1 the rise time of the AOM limited how short the pulses could be made in the data storage experiments, so if shorter pulses are desired lenses with shorter focal lengths must be chosen so that the beam focus is narrower. This will however also decrease the efficiency of the AOM's.

## 6. Acknowledgements

I would like to thank the members of the photon echo group for good support during the work of thesis.

Especially my supervisor Stefan Kröll who allowed me to do this project and who has been supportive along the way.

And also especially my co-supervisor Mattias Nilsson whom I always bugged with questions.

And further the rest of the members in the photon echo group, Lars Rippe and Ingela Roos, for answering questions and for interesting discussions during lunches.

I would also like to thank Leif at cryolab for always find the time to provide me with the liquid helium no matter how late I was in the requests.

I am also grateful for the nice spirit of the atomic physics community here in Lund, which was especially noted during the Tuesday coffee breaks.

Finally my thanks go to my family and to all my friends who have been supportive in so many other fields than physics over the years.

## 7. List of references

- [1] H. Lin, T. Wang, T. W. Mossberg, *Demonstration of 8-Gbit/in.<sup>2</sup> areal storage density based on swept-carrier frequency-selective optical memory*, Opt. Lett. **20**, 1658 (1995)
- [2] M. O. Scully, M. S. Zubairy, *Quantum Optics*, Cambridge University Press, p. 146-157 (1997)
- [3] A. E. Siegman, *Lasers*, University Science Books (1986)
- [4] M. Afzelius, *Theoretical modelling of temporal compression of optical pulses and pulse sequences using photon echoes*, Master's Thesis, LRAP-251, Lund Institute of Technology (1999)
- [5] T. W. Mossberg, *Swept-carrier time-domain optical memory*, Opt. Lett. **17**, 535 (1992)
- [6] L. Levin, *Construction and design of an electro-optically tunable mode-hop free external cavity diode laser*, Master's Thesis, LRAP-261, Lund Institute of Technology (2000)
- [7] N. W. Carlson, L. J. Rothberg, A. G. Yodh, W. R. Babbitt, T. W. Mossberg, *Storage and time reversal of light pulses using photon echoes*, Opt. Lett. **8**, 483 (1983)
- [8] M. Kuldkepp, *Construction and design of a high-power double-pass laser diode amplifier*, Master's Thesis, LRAP-273, Lund Institute of Technology (2001)
- [9] X. Wang, *Photon-echo-based Optical Data Compression Using an External Cavity Diode Laser*, Master's Thesis, LRAP-250, Lund Institute of Technology (1999)
- [10] X. Wang, M. Afzelius, N. Ohlsson, U. Gustavsson, Stefan Kröll, *Coherent transient data-rate conversion and data transformation*, Opt. Lett. **25**, 945 (2000)
- [11] M. Nilsson, L. Rippe, N. Ohlsson, T. Christiansson, S. Kröll, *Initial Experiments Concerning Quantum Information Processing in Rare-Earth-Ion Doped Crystals*, Physica Scripta: Condensation and Coherence in Condensed Matter, Proceedings of the Nobel Jubilee Symposium, p. 178-185 (2002)
- [12] F. R. Graf, A. Renn, G. Zumofen, U. P. Wild, *Photon-echo attenuation by dynamical process in rare-earth-ion-doped crystals*, Phys. Rev. B **58**, 5462 (1998)
- [13] M. Nilsson, *Multi-bit data storage using photon echoes*, Master's Thesis, LRAP-263, Lund Institute of Technology (2000)

## 8. Appendix A

This appendix is included to make future use of the laser diode amplifier presented in [8] easier. It is written in the form of a list of things to check in order to make sure that the incoming laser beam hits the amplifier chip and that it does so with the right focus.

1. The first thing that should be checked is that the outgoing beam from the stand alone amplifier when it is lasing on itself is well collimated. This is easily done by following the beam a long distance to some spot a good distance from the amplifier, all the while monitoring the size to see that it doesn't have a focus somewhere. There are two lenses in the amplifier as can be seen in figure A.1 below. It is basically the same figure over the lens system as can be found in [8].

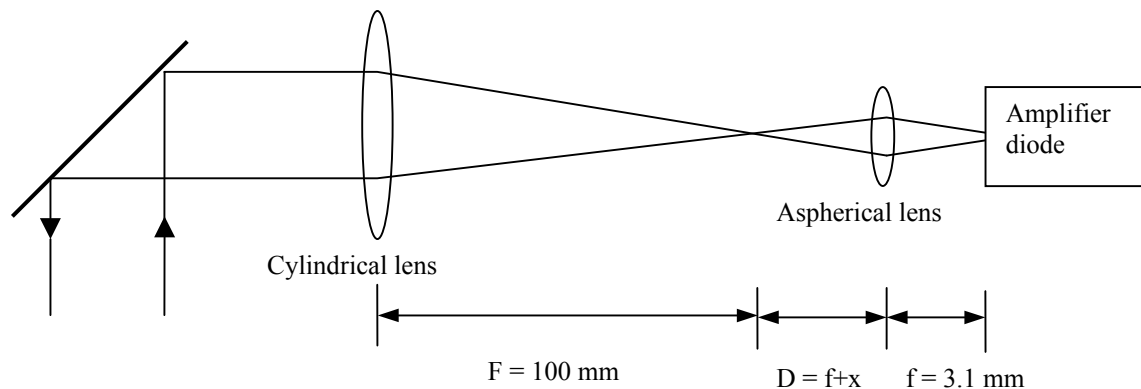


Figure A.1 Schematic over the lens system. It is displayed as viewed from the top.

Moving the cylindrical lens will effect only the lateral dimension but the aspherical will effect both dimensions of the beam cross section. Therefore one must adjust the aspherical first, and then when the height dimension is collimated, the cylindrical lens can be moved to adjust the other dimension freely.

Although it's unknown where the final foci actually are, because of the difficulties if measuring it, it can still be explained where they should be when the amplifier is working as intended. Figure A.2 below shows a close-up of the laser diode chip from both top view and side view.

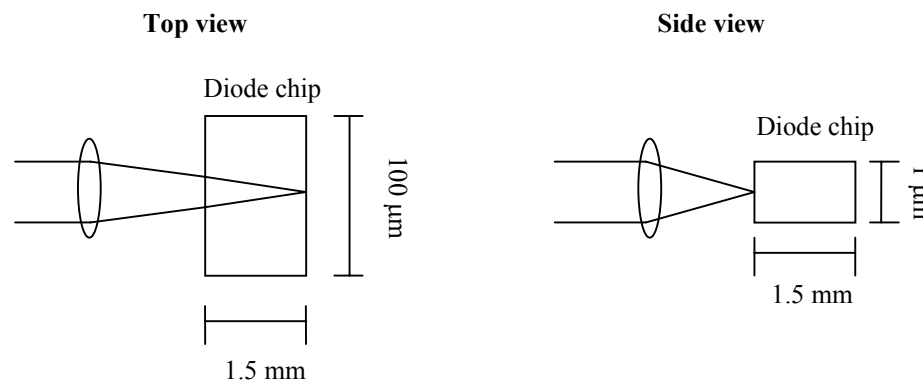


Figure A.2 The top view shows that the lateral focus should be at the back end of the diode chip, so that the injected beam comes from the amplifier as collimated as it went in. The height focus should on the other hand be on the front facet of the diode chip as seen in the side view, because the chip is small enough in this dimension to act as a waveguide

2. Look at the self-lasing amplifier and make sure that the shape of the beam cross section is not tilted in any direction. If it is, there are two things one can adjust. Either the cylindrical lens, which is now mounted on a rotatable holder, or the diode chip itself. This can be done by rotating a copper plate in the back of the amplifier, behind the chip and the temperature stabilisers.
3. Now, the lenses should be reasonably well in place. The final step is to get an amplified beam out when injected with a laser beam. The strategy is to run the amplifier just above its own lasing threshold and to match the amplifier beam with the incoming beam. The two beams should run completely parallel, separated by maybe 0.5 cm, that is almost overlapping. When the alignment was done in the work of this thesis, there were two main spots in the outgoing beam and it appeared to be successful to try and direct the ingoing beam through one of these spots. This means that it will overlap completely with half of the free running beam and the idea is to have the amplified beam come out through the other of the two spots. Note that this process is very sensitive to changes in some of the mirrors and lenses.